A study on deformation behaviour of Cu- Al_2O_3 metal matrix composite with the variation of size and volume fraction of reinforcement particle

A thesis submitted in partial fulfillment of the

requirements for the degree of

Master of Technology

in

Metallurgical and Materials Engineering

By

Sujata Panda

(Roll No- 210MM1250)

Department of Metallurgical and Materials Engineering

National Institute Of Technology, Rourkela

2012

A study on deformation behaviour of Cu- Al_2O_3 metal matrix composite with the variation of size and volume fraction of reinforcement particle

A thesis submitted in partial fulfillment of the

requirements for the degree of

Master of Technology

in

Metallurgical and Materials Engineering

By

Sujata Panda

(Roll No- 210MM1250)

Under the guidance and supervision of

Prof. Bankim Chandra Ray

Department of Metallurgical and Materials Engineering

Department of Metallurgical and Materials Engineering

National Institute Of Technology, Rourkela

2012

National Institute Of Technology

Rourkela

CERTIFICATE

This is to certify that the thesis entitled, "**A study on deformation behavior of Cu- Al_2O_3 metal matrix composite with the variation of size and volume fraction of reinforcement particle"** submitted by **Sujata Panda(210MM1250)** in partial fulfillment of the requirements for the award of Master of Technology in **Metallurgical and Materials Engineering** at the National Institute of Technology, Rourkela is a bonafide research work carried out by her under my supervision and guidance.

To the best of my knowledge, the matter embodied in the thesis is based on candidate's own work, has not been submitted to any other university / institute for the award of any degree or diploma.

Date:

Supervisor

Prof. Bankim Chandra Ray
Dept. of Metallurgical and Materials Engg.
National Institute of Technology
Rourkela – 769008

ACKNOWLEDGEMENT

The equipment and materials used in this investigation were provided or made available by the Department of Metallurgical and Materials Engineering at National Institute of Technology, Rourkela. With the deepest gratitude I wish to thank every person who has come into my life and inspired, touched and illuminated me through their presence.

I avail this opportunity to extend my hearty felt thanks to my guide Prof. B.C Ray, Metallurgical and Materials Engineering for his generous sharing of wisdom, magnificent support, constant encouragement and never ending patience throughout the entire period of investigation.

I also like to acknowledge and express my gratitude to M/s Khusbhu Dash, a magnificent human being who imparted completeness to this thesis from her busy schedule. The support and guidance provided by her is highly appreciable.

I am also thankful to laboratory members of Department of Metallurgical and Materials Engineering, NIT Rourkela, especially, R. Pattnaik, U. K. Sahu and S. Hembram for the extraordinary help I received from them.

I would like to express my deepest gratitude and heartfelt regards to my parents and siblings who have always been supporting me in my studies. Thanks for your love and support!

A part of thanks is due for my precious friend Chandana, Shubhanwita, Arabinda who were always by my side and whose support knows no limit.

Sujata Panda

ABSTRACT

Metal matrix composites are revolutionary materials of future which have endowed the material industry with excellent properties which can be tailored in context to desired applications and requirements. The Cu-Al_2O_3 metal matrix composites apart from resisting softening at high temperatures have applications such as spot welding electrodes, lead frames commutators for starting helicopters, catalysts with a high degree of conversion, coatings with low porosity and high adhesion. In the present investigation Cu–Al_2O_3 micro- and nanocomposites with different volume fractions of alumina (5, 10, 15 and 20 vol. %) were fabricated by powder metallurgy route. The specimens were sintered at different temperatures (850°C, 900°C and 1000°C temperature) to study the effect of sintering temperature on physical and mechanical properties of the composites. These micro- and nano-composites have been characterized using X-Ray diffraction, scanning electron microscopy and atomic force microscopy followed by density, microhardness and wear measurements. Deformation mechanism dominated by dislocation motion has been emphasized comprehensively and critically by changing the particle size and volume fraction of the reinforcement. The mismatch in several physical and mechanical attributes of the matrix and reinforcement entities give rise to misfit strain, thermal misfit, lattice parameter misfit, elastic inhomogeneity misfit. Our investigation focuses comprehensively on thermal misfit in metal matrix composites. The differential elastic modulus of reinforcement Al_2O_3 particle and matrix copper leads to development of misfit strain. It restricts the mobility of dislocation in the matrix leading to strengthening contribution of misfit hardening which is expressed as

$$\tau \propto G\varepsilon^{3/2}\sqrt{rf}$$

Where τ is the misfit strain hardening, G is the shear modulus, is the misfit strain, r is the radius of the particle, f is the volume fraction of the reinforcement. The flexural and compression tests were carried out to investigate the mechanical behavior of MMCs. The thermal mismatch of both entities (matrix and reinforcement) plays a vital role in the thermo-mechanical reliability of the composite. Thermal misfit dislocations at the interface results in generation of strain field at the particle-matrix interface. The amount of geometrically-necessary dislocation density generated in the matrix- reinforced particle interface can express as

$$\rho_g \leq \frac{12}{\sqrt{2}}\frac{\Delta\alpha\Delta T}{r_p b}\frac{f}{(1-f)}$$

Where ρ_g dislocation density, Δα is the difference in thermal expansion coefficient, ΔT is the change in temperature; f is the volume fraction of the reinforcement $\sqrt{2}\ r_p$ is the dislocation loop radius. The specimens of Cu – 5 % Al_2O_3 having particle size (10 µm, <50 nm) were treated at -80 °C for a time period followed by immediate exposure at +80 °C for the same period of time. The thermal shock procedure was also followed in the reverse order. The flexural tests were conducted at room temperature maintaining a span length of 26mm and strain rate of 0.5 mm/mm min. An attempt was made to emphasize on the response of strengthening effect of particle reinforced composite with various thermal shock treatments (up and down cycle). The in-situ flexural tests were carried out at +250°C, +100°C. The strain hardening effect, ductility, flexural moduli were reflected from the three point bend test results.

The following observations have been made from the present investigation:

Micro-composites

I. Volume fraction of the reinforcement: With increases in reinforcement content particle clustering increases.

II. Sintering temperature: $CuAlO_2$ phase appears from Cu_2O at 1000°C sintering temperature. Particle clustering decreases with increases in sintering temperature. Annealed twins are more likely to observed in the micro composites sintered at 900°C less likely at 1000°C. With increases in sintering temperature densification values of the micro-composites increases.

III. Mechanical behavior: Density decreases with increases in reinforcement content. Increases in the reinforcement content increases the micro hardness values. Hardness values decreases with increase in sintering temperature from 900°C to 1000°C. wear resistance decreases with increase in reinforcement volume fraction. With increases in reinforcement content the ultimate compressive strength decreases. Cu–15 % Al_2O_3 composite with 10 micron have highest ultimate compressive strength. Maximum flexural strength decreases with increases in alumina content. . Particle pullout, interface de-cohesion, and matrix cracking are the dominant failure phenomenon.

IV. Thermal shock: Maximum flexural strength increases for both up and down thermal shock treatment. Particle cracking is the dominant failure mechanism in the down thermal shock whereas up thermal shock treated specimens fail by interfacial de-cohesion.

V. In-situ high temperature TRS- At high exposed temperature maximum flexural strength increases. As the test temperature increases from 100°Cto 250°C the flexural strength decreases by 33%.

Nano-composites

I. Volume fraction of the reinforcement: Increase in the volume fraction of the reinforcement sintered density decreases.

II. Sintering temperature: At high sintering temperature hardness value decreases with increases in sintering temperature.

III. Mechanical behavior: Hardness values increases with increases in the reinforcement content. Ultimate compressive strength of the nano composites were decreases with increase in the reinforcement content. Strain hardening exponent also decreases with increase in reinforcement content. Cu–7 % Al_2O_3 nanocomposite provides the maximum bending strength. Mixed (cleavage and dimple) mode failure of the nanocomposite has been observed.

IV. Thermal shock: Maximum flexural strength increases for both up and down thermal shock treatment. Matrix deformation is the predominant failure mechanism for down thermal shock. In up thermal shock treated sample interfacial cavitation is the principle damage mechanism.

V. In-situ high temperature TRS: At high exposed temperature maximum flexural strength increases. As the test temperature increases from 100°Cto 250°C the flexural strength decreases by 20%

The present research confirms that the deformation behavior of particle reinforced metal matrix composites are affected by particle size, volume fraction of the reinforcement, particle distribution. Particle cracking, particle/matrix interface de-cohesion, particle pullout and localized melting are some of the failure mechanisms operational in MMCs which lead to the premature and unpredictable failure of composite materials.

Keywords: Cu-Al_2O_3, Micro composite, Nano composite, Deformation, Thermal misfit dislocation, Thermal shock.

Content

List of Figures

List of Tables

Chapter 1
Introduction

Chapter - 1
Introduction

1.1 Introduction

Metal Matrix Composites (MMCs) have emerged as a class of excellent engineering materials in the modern era suitable for structural, aerospace, defense, automotive, electronic, and thermal and wear applications owing to their advantages over the conventional monoliths. Copper has been extensively used as matrix because of its superior heat and electrical conductivity. On the contrary pure copper does not have acceptable mechanical properties [1]. The mechanical strength of copper can be improved either by age hardening or by particles dispersion strengthening. The age-hardenable copper alloys are prone to precipitate coarsening at high temperatures which results in degradation of strength of the material [2]. Matrix strengthening can be done by incorporation of reinforcement like continuous or discontinuous fibers, whiskers, wires and particulates. The reinforcements are generally ceramic; which can be in the form of oxides, carbides and nitrides. Fine ceramic particles as oxides or carbides in copper enhance the strength and hardness and retain the properties at high temperature also, causing only a small degradation in electrical conductivity. The major requirements for the particle dispersed composites are thermodynamic and chemical stability of the reinforced particles, low diffusivity and low solubility in the matrix, high interfacial energy and closeness of thermal coefficient of expansion of the matrix and reinforcement. Al_2O_3 raises the recrystallization temperature and strength at elevated operating temperature by grain boundary pinning of the copper matrix [3]. Orowan strengthening mechanism, Hall Petch relation, Taylor work hardening equation are some of the best functional tools to explain the strengthening mechanisms of MMCs [4].

Introduction

The highlights of MMCs are high strength to weight ratio and high stiffness per unit density as a result the service performance is enhanced. The lowering in structural weight, increase in creep strength, and enhancement in wear resistance and decrease in thermal expansion coefficient of the composite as compare to base metal [5, 6, 7] further make it a excellent candidate material for critical applications. The unique physical properties are no moisture absorption, non-flammability, high electrical and thermal conductivities and resistance to most radiations. The Cu matrix composites are extremely used in thermal management industries, wear resistant and heat resistant materials. A large variety of thermal management components include power amplifier heat sinks, heat sinks for integrated circuit breakage, printed circuit board cores, cold plates, chip carriers, heat spreaders and rectifier packaging [8]. The wide applications of Cu – Al_2O_3(p) material are for relay blades, railway overhead current collector systems, homopolar machines ,resistance welding electrodes, electrical connectors, continuous casting mould and first wall of nuclear reactors such as ITER (International Thermonuclear Experimental Reactor) [4,9].

Discontinuously reinforced metal matrix composites has been produced by various processing route such as melt casting, powder metallurgy, spray deposition, mechanical alloying, SHS (self propagating high temperature synthesis). Among these powder metallurgy route is the efficient one because of homogeneous distribution of reinforcement in the matrix, less chance of undesirable triple phase formation and minimization of detrimental interfacial reaction, minimization of reinforcement segregation, good interfacial bonding, near net shape product fabrication [7, 10, 11]. In case of particle reinforced MMCs the service life of the material

strongly influenced by type and behavior of matrix materials, individuality of the reinforcement, interface characteristics, reinforcement clustering and formation of interfacial products. the coefficient of thermal expansion (CTE) mismatch between the reinforcement and the matrix develops a high residual stress or thermal stress, which leads to the low tensile ductility of the composite [12,13] The driving phenomena to generate dislocations in MMCs are misfit strain, thermal misfit, allotropic misfit, lattice parameter misfit and elastic inhomogenity misfit [14, 8]. In case of solid solution strengthening the dislocation motion gets impinged by elastic interaction between the dislocation and solute atoms as well as by altering the energy of stacking fault [15]. . The crucial parameter effecting the fracture of a particle reinforced composites are size, shape, concentration and spatial distribution of the reinforcement, the concentration of impurities present in the constituents phase of composites, thermal and chemical exposure environment and particular reinforcement size matrix alloy combination [16]. A clean metallurgical interface (free from interfacial phase) is desired for effective reinforcement strengthening [17].

1.2 Research objective

The primary objective of this research was to evaluate the effects of sintering temperature on physical and mechanical property of the composite. The volume fraction and particle size of the reinforcement was varied at various sintering temperatures in order to investigate the effect of particle size and volume fraction on the durability and reliability (interfacial integrity) of the composite. A critical and comprehensive understanding of the microstructural evolution of the composites was investigated through scanning electron microscopy (SEM). Physical condition of the interface of Cu-Al_2O_3(p) composite and the source of damage nucleation with the variation of

Introduction

Al_2O_3 content and size, sintering temperature were investigated from SEM micrograph. X-Ray diffraction, density, hardness, wear test, compression strength, flexural strength and failure mode of the composite were elaborately investigated to arrive at a correlation of particle size – reinforcement content - process parameter – interface profile – microstructure - mechanical properties - reproducibility correlation of the composite. Subsequently the microscopic deformation behavior of Al_2O_3 reinforced Cu metal matrix composite was investigated by compression and 3-point bend test coupled with fractography. A set of samples were subjected to a thermal shock of -80°C to +80°C and vice versa for different period of exposure and 3-point bend test was done. Thermal conditioning of the 3-point bend test samples were done at +80°C and -80°C for 1 hour. In-situ 3-point bend test was done at different exposed temperatures to study the post sintering effect on the composites. The fracture surfaces were analyzed under SEM in order to study the change in mechanical behavior and failure mode of the composites at various thermal shock responses. A general idea about the interfacial bonding, phase stress generated and thermal misfit dislocations generated as a consequence of thermal mismatch which was drawn from the fracture surface of SEM micrographs have been especially brought under consideration to correlate the experimental results with microstructural evidence.

Chapter 2

Literature Review

Literature Review

2.1 Background of metal matrix composite

Demand to increase the service life of advance military systems provide a primary motivation for the development of metal matrix composites (MMCs) [18]. In early 80s demand of high strength metallic material expanded the scope of MMCs. The discontinuously reinforced MMCs increased the performance of the equipments. In the late 1980s National AeroSpace Plane (NASP) in United States designed a continuously reinforced composite which increases the durability and reliability of the composites [8].

2.2 Metal matrix composite

Metal matrix composites (MMCs) can be described as an excellent candidate materials for advanced applications in which with one or more reinforcement phases is incorporated in a continuous metallic phase (matrix). The aim of such a composite material is to enhance the durability and reproducibility of the desire product by selectively enhancing the complimentary properties, and masking the detrimental properties of the matrix and the reinforcement.

As metals exhibit low strength, the strengthening of metal matrix composites can be achieved by incorporation of fine ceramic particles or nucleation of precipitates within the metallic matrix. For effective strengthening the reinforced particle must be closely spaced (< 1 micron). Precipitation hardened system exhibit higher strength at room temperature. With increase in operational temperature the precipitate gets dissolved in the matrix. As oxides particles are more stable at high temperature, particle dispersion composite shows superior mechanical property at elevated temperature. The development objectives for metal matrix composite materials are: increase in yield strength and tensile strength at room temperature and

above while maintaining the minimum ductility or rather toughness, increase in creep resistance at higher temperatures compared to that of conventional alloys, increase in fatigue strength, especially at higher temperatures, improvement of thermal shock resistance, improvement of corrosion resistance, increase in Young's modulus, reduction of thermal elongation, taliorable coefficient of thermal expansion [19].

2.3 Conventional sintering

Sintering is a method to consolidate powder particles at high temperature in a furnace to below its incipent fusion temperature until the particles adhere to each other. During sintering particles are bonded together by diffusion of atoms to minimize the surface energy. In case of conventional sintering the compact mass are heated to a point, below the melting temperature of the matrix, where the atoms can diffuse. Changes that occur during the firing process are related to (1) changes in grain sizes and shape, (2) changes in pore shape, and (3) changes in pore size. Diffusion is a temperature driven phenomenon which requires minimum energy to start off. This is caused by a chemical potential gradient where atoms move from a higher chemical potential region to a region of lower chemical potential. The different paths the atoms take to get from one spot to another are known as the sintering mechanisms. Arrhenius relation describes the activation energy required for thermal diffusion is stated as:

$$D = D_0 e^{\frac{-Q}{RT}} \quad \text{.....(2.1)}$$

where *D* is diffusivity, *Do* is the diffusivity pre-exponential, *R* is the universal gas constant ,and *T* is the operating temperature and *Q* is the activation energy for self-diffusion (equal to 0.145

Tmelt in Kelvin). The particle surface energy is inversely related to the particle diameter by a Laplace equation;

$$\sigma = \gamma\left(\frac{1}{R_1}+\frac{1}{R_2}\right) \quad \text{(2.2)}$$

where γ is the surface energy, and *R1* and *R2* are the radii of curvature of the surface. Smaller particles have higher surface energies per unit volume. As atoms diffuse to the contact region, a neck forms between the particles. Atoms transport from high energy convex particle surfaces to concave surfaces,necks.Fusing increased surface area as a result pore volume and density of the compact remains almost constant.(4-5% shrinkage, relative density 0.5-0.6).

After initial neck formation, atoms continue to diffusion of atom to the neck region, which increases the radius of curvature leads to slow down the sintering process as the driving force is reduced. In the intermediate sintering stage, pore volume is decreased and pore structure changes from being irregular to an interconnected cylindrical structure along the grain boundaries. During intermediate stage of sintering, densification, pore rounding, and grain growth occur simultaneously. Decrease in pore volume makes the pore structure unstable and at the final stage of sintering, the pore structure collapses into spherical isolated pores. Grain growth and isolated pores at late stage of sintering can slow the rate of densification.

The six common operative mechanisms during sintering are **[20]**:

1. Surface diffusion – Diffusion of atoms along the surface of a particle, involves the rearrangement of particles to form a neck without any densification. In case of surface diffusion atom usually move from the site of a surface defect to another defect site by the random motion of the atom. In neck formation in surface diffusion, atoms reduce the curvature of the neck and

thereby reduce the surface energy. Surface diffusion is the dominating mechanism at low temperatures in most metals, including nickel.

2. Vapour transport –Evaporation occurs from a particle surface and atoms move across the pore space and condensed on a different surface. Metals with high vapor pressure undergo evaporation-condensation surface diffusion.

3. Lattice diffusion from surface – atoms from surface diffuse through lattice.

4. Lattice diffusion from grain boundary – Grain boundary atoms diffuses through lattice

5. Grain boundary diffusion – Diffusion of atoms takes place along grain boundary. Grain boundary diffusion is important in most polycrystalline metals as it is more energetically favorable than diffusion through the lattice.

6. Plastic deformation –Plastic deformation corresponds to the glide and climb of dislocations due to stress at the neck and absorption of vacancies during pore size reduction. Plastic flow is important during the heating stage (especially for compacted powders with high dislocation density) but decreases as dislocations are annealed out of the particles.

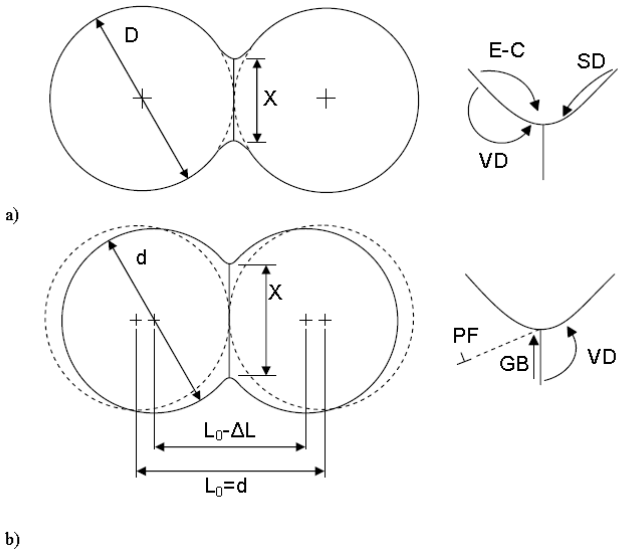

Fig. 2.1 Idealized two sphere sintering model. The surface transport mechanisms (a) evaporation-condensation (E-C), volume diffusion of atoms from the surface to the surface (VD), and surface diffusion (SD) lead to neck formation, but not to a change in the particle centers.

The bulk transport mechanisms (b), plastic flow (PF), grain boundary diffusion (GB), and volume diffusion (VD) are responsible for changes in the particle centers (densification). Adapted from German [20, 21].

There is a strong dependence on inverse particle size, meaning that smaller particles sinter more rapidly. Also, surface diffusion and grain boundary diffusion are more important for smaller particles. There is an exponential dependence on temperature which can be inferred from the neck growth equations.

$$\left(\frac{X}{d}\right)^n = \frac{Bt}{d^m} \quad \textbf{(2.3)}$$

where *X* is the neck diameter, *d* is the particle diameter, *t* is time, and *B*, *m*, and *n* are a collection of material and geometric constants. Therefore small changes in temperature are expected to have large effects. Fine particles sinter much faster than the coarse one because of larger surface area and smaller diffusion distance of the former. The rate of densification can be expressed as

$$\frac{d\rho}{dt} = \frac{c}{s^n} e^{\frac{-Q}{RT}} \quad \text{.....(2.4)}$$

Where ρ is the density, C and n are constants, s is the particle size ,Q is the activation energy for sintering, T is the absolute temperature and R is the universal gas constants. Grain boundaries have a strong effect on sintering; limited grain growth promotes densification. The mean grain size is a function of time:

$$G^g = G^g_o + Kt \quad \text{.....(2.5)}$$

where *Go* is the initial grain size and *K* is a thermally activated parameter and *g* is the grain growth exponent. Grain growth increases as the pores either coalesce or as porosity is eliminated. Densification is slowed and can be stopped by trapped gas in the pores when the surface energy of the pore is equal to the gas pressure:

$$4\gamma = P_g\, d_p \quad \text{.....(2.6)}$$

where P_g is the gas pressure of the pore and d_p is the pore radius. Difference in the pore curvature causes smaller pores to be absorbed into larger pores in order to reduce the surface energy. For achieving full density sintering requires a vacuum medium.

2.4 Strengthening mechanisms of MMCs

The different strengthening mechanisms which improve the strength of the composites are:

2.4.1 Direct strengthening

In case of direct strengthening the load from the matrix get directly transfer to the reinforcement. As the reinforcement is stronger than matrix it increases the strength of the material [22]

2.4.2 Lattice friction strengthening

The crystalline nature of the lattice itself inhibits the dislocation motion. This is called lattice friction or Peierls stress. The Peierls stress for FCC metal is 10^{-5}G, for HCP metal it is $5X10^{-5}$G and for BCC metal it is about 0.1-1G.

2.4.3Solid solution strengthening

Solid solution strengthening impedes the dislocation motion physically by elastic interaction of the strain field between the dislocation and solute atoms and chemically by altering the stacking fault energy. Strengthening effect of solute atoms increases with square root of concentration in dilute solutions.

$$\tau = \tau_{\circ} + k\left(1 - \frac{T}{T_c}\right)\sqrt{\frac{W^3 c}{Gb^9}}$$

……..…….(**2.7)**

Where τ is the stress for which dislocation motion occur, T is the temperature, Tc is the temperature based on strain rate, W is the dislocation solute interaction energy, c is the concentration of mole fraction.

2.4.4 Dispersion as Orowan strengthening

The incorporation of reinforcement to the pure metal matrix improves the strength by dispersion hardening. In case of Orowan strengthening mechanisms the glissile dislocations interact with the hard particle. Under an applied stress dislocation pinned out by two particle in its glide plane and bow out.

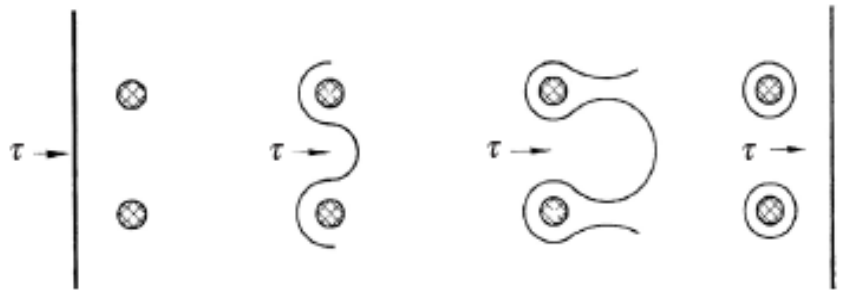

Fig. 2.2 The Orowan model.

At a critical stress two adjacent bowed segment joined leaving a dislocation shear loop around the particle. The increase in flow stress to bypass particle of interparticle spacing H is

$$\tau \approx \tau_f + k\frac{Gb}{H} \quad \textbf{(2.8)}$$

Where τ is the flow stress and τ_f is the stress required to move a dislocation in obstacle free crystal. For uniformly distributed spherical particle of volume fraction f and radius r_p given as

$$\tau \approx \tau_f + k\frac{Gbf^{1/3}}{2r_p} \quad \textbf{(2.9)}$$

The reinforcement size and distribution affect the strengthening process of the composite[23].

2.4.5 Work hardening

Because of the presence of stress field around each dislocation the motion of the dislocation through the lattice is restricted by the other dislocations which is responsible for the work hardening effect in metals [22, 24]. As large number of thermal misfit dislocations are generated during processing and servicing of the discontinuously reinforced composite due to the mismatch of coefficient of thermal expansion. Metals like Cu which has low stacking fault energy work hardens more rapidly than metals like Al because the widely spaced partial dislocation are more susceptible to form sessile dislocation segments[17].

$$\tau \approx \tau_f + kGb\sqrt{\rho} \quad \textbf{(2.10)}$$

ro(ρ) is the dislocation density in units of total dislocation length per unit volume.

2.4.6 Grain boundary strengthening

Gran refinement is an important strengthening increases the fracture toughness and strength at low temperature. The magnitude of strengthen is determined by Hall- Petch relationship:

$$\tau = \tau_f + kd^{\frac{-1}{2}} \quad \textbf{(2.11)}$$

Where d is the grain size. The hall petch relationship describe the strength increases with decreses in grain size . But for very small particle(<10 nm) the relationship does not holds good. A large difference of elastic property between the reinforcement and matrix particles develop high dislocation density in the interfacial region[25].

Effect of size on the strengthening mechanisms

As nano particle are very small in size, easy accommodation of the particle in the matrix occur which increases the compatibility and close proximity between particle and matrix. Easy accumulation of dislocation occur at the vicinity of reinforced particle, dislocation gets pinning down more easily leading to dislocation arrest in the vicinity of the particle.

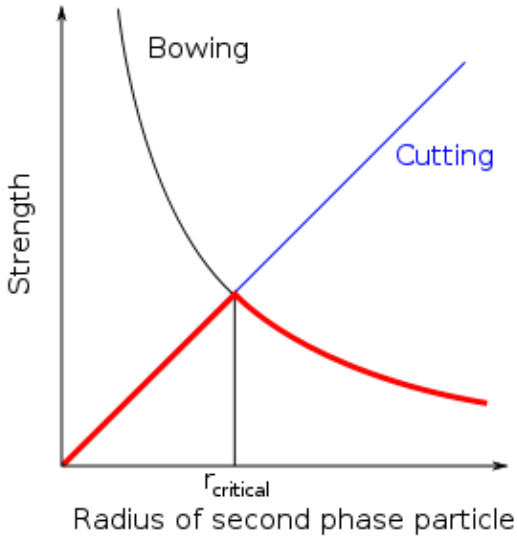

Fig 2.3 Plot showing the strength increases with increases in particle radius, after a certain limit strength decreases with further increases in particle radius.

Since the strengthening potential for dislocation looping around non coherent particle is less then that associated with particle cutting process such alloys are not among the structural material

Effect of vol% of the reinforcement content

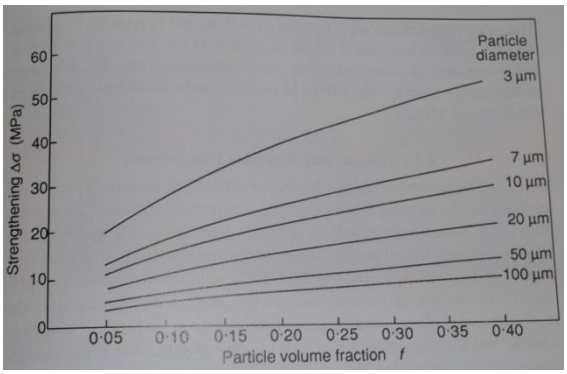

Fig 2.4 Plot for composite strengthening value with different volume fraction of reinforcement for different particle size.

Wit increases in volume fraction of reinforced particle the mechanical property gets enhanced.

$$\Delta\rho = 12\,\frac{\Delta\alpha\Delta T f}{bd} \quad \text{.....(2.12)}$$

$$\Delta\sigma_{YM} \sim Gb\sqrt{\rho} \quad \text{.....(2.13)}$$

Δ ρ is increases in dislocation density, ΔαΔT represents thermal misfit strain, f is the vol. % of reinforcement, b corresponds to the burger vector, d is particle size and G is shear modulus

Δ YM = Strengthening (Mpa). With increases in volume fraction of the particle the dislocation density around the particle increases according to the equation 2.12. This leads to the pinning of dislocation which increases hardness of the composite [12].

2.5 Failure mechanisms in metal matrix composites

In case of metal matrix composite the failure of material occurs by interfacial de-cohesion, reinforcement particle cracking, void nucleation at the pole of the reinforced particle [26]. Interfacial de-cohesion is the primary mode of damage mechanisms for small size (3 µm – 6 µm) reinforced particle whereas large size (10µm-23 µm) reinforced particle composites fail by

particle cracking. For most of the materials, room temperature damage is prevalent by reinforcement fracture but the damage mechanism changes to void nucleation by interface decohesion at a temperature around 200°C and above. [27]. At high temperatures (300°C) damage occurs by matrix voiding in the vicinity of reinforced particle and the interface de-cohesion. At high operating temperature reinforcement particle played a minor role in the failure process, as the plastic strain being accumulated by the extremely ductile matrix.

At clustered region, the amount of reinforcement volume fraction is larger which imposed a higher plastic constraint to the plastic deformation of the ductile matrix. Due to this large hydrostatic stress developed in clustered regions, which increases the maximum principal stress in the particle leading to the early damage of the composite by reinforcement particle cracking. The necessary condition for interface de-cohesion is that the local elastic strain energy released during de-cohesion should be sufficient to create the new free surface at the interface. The above condition holds good for particle of few length of nm or smaller [21,28]. So most of the metal matrix nanocomposites fail through the interface de-cohesion.

The final failure takes place by the sudden coalescence of the voids through the metallic matrix which get nucleated at the matrix-reinforcement interface resulting in matrix rupture. The critical conditions for void coalescence are microstructure of matrix, test temperature and loading conditions.

2.6 Fractography of metal matrix composite

Fracture	Ductile fracture	Brittle fracture

Characteristics		
	Tearing of metal	Rapid crack propagation
Plastic deformation prior to fracture	Appreciably gross plastic deformation	Minimal or no plastic deformation prior to fracture
Energy consumption	Considerable amount of energy consumed and propagate in a high index plane	Less energy consume then that of ductile fracture and propagate in a low index plane
Fracture surface	Perpendicular to the maximum tensile stress	Generally flat type fracture surface
	Micro void formation and coalescence	fracture may be trans-granular or inter-granular

Table. 2.1: A comparison between fracture features of ductile and brittle mode of fracture.

Most of the structural material fails by a process known as micro-void coalescence. The micro-voids nucleates at region of localized strain discontinuity like second phase particles, inclusion and grain boundary dislocation piles up. As the strain in the material increases microvoids grow, coalescence and form a continuous fracture surface. Broken or decohered particles are present at the center of each large dimple. This evident that matrix material in the void undergoes extensive plastic deformation by shear and is drawn out to form a sharp shear lip.

The wall of the dimples around the reinforcement particle covered with fine striations. Theses striations are produced by serpentine glide which appears when slip planes with in the material intercept the unconstrained surface of the void [29]. Fracture surface reveals that the more number of dimple population are present having different diameter.

Presence of dispersed second phase particles in the matrix nucleated micro-voids as plastic deformation becomes localized in the matrix around the particles. Void coalescence occurred by the progressive growth and impingement of theses micro-voids and the fracture surface shows dimples of different diameter. The largest dimple forms around the reinforced particle. The size of the dimples on a fracture surface depends on the number and distribution of micro-voids that are nucleated. When the nucleation sites are less (reinforcement vol. % is less) and widely spaced the micro-void grow to a larger size. Small dimples are formed when numerous nucleating sites are activated and the micro-voids join before they have an opportunity to grow to a larger size[30]. Fracture under uniaxial tensile load results in equiaxed dimples. Oval-shaped dimples are observed on the wall of large elongated dimples. Oval dimple is formed when a small surface void intersect the wall of a larger void.

Cleavage fracture

Cleavage fractures are the low energy fracture propagates along low index crystallographic plane known as cleavage plane. Cleavage fracture surface is flat and featureless. Cleavage steps, river patterns, feather marking, chevron (herring bone) patterns, tongues are the different type of cleavage fracture. Cleavage fracture initiate on many cleavage planes parallel to each other. On the propagation of fracture active cleavage planes joins together that form progressively higher

cleavage step which is known as river patterns. The directions of river patterns propagation signify the direction of local fracture [30].

Feather marking are a fan shaped array of very fine cleavage steps on a large cleavage facet. Tongues are occasionally observed on cleavage fracture. They form when a cleavage fracture deviates from the cleavage plane and propagates a short distance along twin orientation. [30]

2.7 Thermal stress

The thermal stress or phase stress generate in the metal matrix composite due to the difference in coefficient of thermal expansion of metal and reinforced particle. The thermal stress also know as internal stress of lock in stress. The thermal stress depends on reinforcement volume fraction, morphology of the reinforcement, matrix crystallographic texture, porosity, possible voids, loading conditions, state of stress. The thermal strain , develops at the interface of a discontinuously reinforced MMCs due to thermal stress is expressed as

$$\varepsilon = \delta\alpha\ \delta T \quad \text{.....(2.14)}$$

Where δα is the difference between the thermal expansion coefficient for the reinforcement and the matrix and δT is the range of temperature experienced during the processing. The thermal stress generates tensile and compressive stress on matrix and reinforcement respectively [31]. The generated thermal strain may exceed the local yield strain of matrix – reinforcement interface which will leads to the damage accumulation at the interface. The resultant phenomena of thermal stress are particulate fracture, de-bonding and cracking in the matrix –reinforcement interfaces, failure in the matrix via micro-void coalescence and shear fracture of the matrix which detoriate the composite property[32].The above failure mechanisms act as the relaxation

phenomena, lowers the internal strain energy and entropy of the composite [31,33]. The strength- weakening of the composite normally occur which is directly proportional to the magnitude of Δα ($\alpha_{composite}$- $\alpha_{reinforcement}$) [34]. The undesirable effects of the residual thermal stress are decrease in fatigue resistance, accelerated stress corrosion and shape detoriation[35].

In metal matrix composite having large thermal strain the plastic deformation is more likely be non-uniform and it is localized [23]. The strengthening (Δ) in the metal matrix in a particulate reinforced MMCs can be determined by

$$\Delta\sigma = Y\mu b\sqrt{\rho}$$

…….(2.15)

where is the constant of order 1, b is the burger vector, μ is the shear modulus of the matrix and ρ is the average dislocation density generated due to the CTE mismatch of the matrix and reinforced particle [20]. When the matrix metal deform plastically internal stress arises as a result of the elastically deformed particulate resisting the plastic flow of the matrix. This internal stress is reffered as back stress which can be considered as characterization of damaged particles will be valuable in improving processing procedures and in understanding deformation and failure of MMCs. At the last stage of deformation matrix softening is the predominant phenomenon because of fragmentation of reinforced particles [23].

2.8 A bird's eye-view of the literature surveyed

Author name	Finding
M. Kubota , P. Cizek, W.M. Rainforth [36]	Uniform distribution of the reinforced particle in the metal matrix enhances the mechanical properties of the composite
X. L. Zhong, W. L. E. Wong [37]	The increases in strengthening of metal matrix composite with increases in reinforcement can be attributed to 1)Orowan strengthening, 2) Grain refinement, 3) Formation of internal thermal stress due to the different coefficient of thermal expansion, 4) Effective load transfer between the matrix and the reinforcement and 5) Hardening due to the misfit strain between the particle and matrix
L. Lu, M.O. Lai, G. Li [38]	With increases in volume fraction of the hard particle density decreases because densification of hardened powders by cold compact becomes more difficult
R.W. Hertzberg[39]	At high operating temperature plasticity increases due to dislocation annihilation or activation of dislocation motion by a mechanisms other than glide like climb.
A.A. Mazen[40]	Plasticity of the metal matrix composite material increases by stress relaxation at matrix-particle interfaces and enhancement

	of recovery processes at theses interfaces
D. Zhao, F.R. Tuler, D.J. Lloyd. [41]	Interfacial decohession is the primary mode of damage mechanisms at high temperature and particle cracking occur at low temperature.
F. Shehata, A. Fathy, M. Abdelhameed,S.F. Moustafa [42]	In situ fabrication of Cu – Al2O3 nano composite by mechano-chemical route. The hardness of the composite increases with increases in vol% of reinforcement content . Alumina nano particle increases the hardness by impeding the movement of dislocation and restricting the grain growth of Cu matrix. $CuAlO_2$(Spinel) third phase product forms in Cu-Al_2O_3 nano composite improves the bond between Cu and alumina.
R. Ritasalo, X. W. Liu[43].	Internal oxidation gives the finer size alumina and uniform distribution due to which hardness values increases The small alumina particle act as a obstacle for the dislocation motion.
M Barmouz, M K. B. Givi, J. Seyfi, [44]	Pure copper reinforced by SiC particles have higher wear resistance in comparison with unreinforced pure copper.
Zhu Jianhua, Lei Liu, Bin Shen, Wenbin Hu [45]	Increase in reinforcement content in the matrix increases the wear resistance of the composite material

A. Levy, M. Papazian[46]	The residual stress leads to the inequality of the tensile and compressive stress-strain curve
E.U. Lee [47]	The differential CTE mismatch induced stress and strain have maximum value at the reinforcement particle/ matrix interface and decreases with distance from the interface. Interface is the potential site for damage initiation.
Y. D.Haung. N. Hort [48]	Post thermal cycling leads to the decress in hardness due to matrix overaging and recovery.
P.Agrawal, C.T. Sun[49]	On cooling from the processing temperature to room temperature the metal phase experience tensile stress whereas ceramic particle experience a compressive stress.
P Agrawal, K. Bowman, CT Sun[50]	At the metal-ceramic interface high tensile stress generated during composite processing. This leads to the interface debonding.
M.Taya, K.E. Lulay, D.J. Lloyd[23]	The strengthening of a metal matrix composite was attributed by punched out dislocation due to differential CTE mismatch strain and backstress.
Hassan SF Hassan, M.Gupta	The reinforced particle refines the grain size of the matrix by pinning the grain boundary area and providing the site for

[51]	nucleation during recrystallisation.
S. F. Moustafa, Z. Abdle-Hamid, A.M. Elhay[1]	Compressive fracture occurred at an angle of 45◦ which is a indication to the shear mode of fracture. Good adhesion between the particle and matrix increases the densification results in increases in the compressive strength value.

Chapter 3

Experimental Details

3.1 Introduction

The aim of this research was to investigate the effect of sintering temperature on the physical property of the composite and the deformation behavior of the Cu-Al_2O_3 metal matrix composite with the variation of the reinforcement content and size. An attempt was made to correlate the effect of thermal shock on mechanical properties of the Cu- Al_2O_3 composite. This chapter deals with the experimental practice as adopted in the present project work. The equipments utilized throughout the project work have been listed in table -1, indicating their technical specifications and the unique applications in details. The phase identification was done from the X-ray diffraction analysis where as microstructure of the composites were observed by scanning electron microscopy. The physical parameters were analysis from density and hardness values. In order to study the deformation mechanisms the specimen having different volume fraction and particle size of reinforcement were subjected to wear, compression and 3-point flexural tests. Some selected numbers of samples were chosen in order to analysis the effect of thermal stresses on the metal matrix composite.

3.2 List of equipment used

Sl. No	Name of the equipment	Technical specification	Application
1	Particle size analyser	Malvern, Mastersizer Range – 0.05 - 550μm	For estimating the particle size range of copper powder powder as well as Al_2O_3 powders.

3	Uni axial cold compaction machine	SoilLab Type: Hydraulic Max. Load: 20 tons	For production of green test specimen for study of sintering phenomenon, compression test specimen and 3-point bend test specimen.
4	High temperature atmosphere controlled tube sintering furnace	Naskar & Co. product Vacuum and Controlled atmosphere(N2 and Ar) Max. temp.: 1750^{o}C Dimensions: Ǿout-85mm, Ǿin-75mm	Used for sintering green pellets, in Ar atmosphere at various sintering temperatures, for different period of time at different heating rate.
5	X-Ray Diffractometer	Philips Analytical XRay X'Pert-MPD system Type: PW3040 2θ range: 0^{o}-160^{o}	For phase analysis, crystal structure determination and the intensity of the present phase.
6	Scanning electron microscope(SEM)	JEOL JSM-6480LV	Surface analysis of the sintered specimen, Compositional analysis, Fractography study.
7	Muffle furnace	Make: Wild Barfield Model: HT25 Max. temp.: 1550^{o}C	For exposing the samples to +80^{o}C, an elevated temperature.

8	Ultra low chamber	Make: S.D. Scientific Industries Ultra low chamber Range: +50^{o}C to -80^{o}C	Treating the samples at -80^{o}C, a low temperature.
9	Universal testing machine	INSTRON-5967, Capacity- 30KN	To carry out the 3-point bend test at room temperature and insitu high temperature
10	Universal testing machine	in Instron- SATEC series servohydraulic machine Capacity-600KN	For compression testing of the composite specimens
11	Hardness tester	Leco Microhardness Tester LM248AT	For the microhardness determination of the MMCs
12	Wear Tester	Ball-On-Plate Wear Tester TR-208 M1	To determine the wear behavior of the conventional sintered specimen
13	density mesurement Kit	Contech CB series	For mesuring the density by Archemedes method.

Table 3.1: List of equipments used during the research work

3.3 Sample fabrication

3.3.1 Raw material

Copper powder from Loba Chemie with an average particle size of 11μm and purity- >99.7% was used as the matrix material. Alumina powder from Sigma Aldrich with an average particle size of 10μm and < 50 nm were selected as the reinforcement materials. The particle size distribution was analyzed using a Malvern, Mastersizer laser scattering particle size distribution analyzer. The powders were suspended in water, poured into the analyzer, and 3 measurements were taken while the reservoir was stirred and agitated ultrasonically. The morphology of the particles was investigated using a JEOL 6480 LV SEM.

Fig. 3.1 Malvern particle size analyzer

3.3.2 Blending

Micro-composites were prepared by mixing and blending commercial Cu powders with various volume fractions of alumina powders (5, 10, 15 and 20 vol. %). The nano-alumina powders were added to copper matrix in a range of composition of 1, 3, 5, 7 vol %. The mixing was done by hand blending method by mortar pestle for 1 hour. For homogeneous mixing, the powders were blended in a centrifugal movement abrasion tester(Fig. 3.2) for 13 hours at a speed of 260 rpm.

Fig. 3.2 Centrifugal rotating blender

3.3.3 Compaction

The blended powders were compacted into 15 mm diameter pellets in an electrically operated uni -axial cold compaction machine (Soil Lab, illustrated in Fig 3.3) at an applied pressure of 700 MPa. A stainless steel die of internal diameter 15mm was used for this purpose. To prevent the specimen from sticking on to the walls of the die zinc stearate was used as a die lubricant during compaction of the pellets. In order to carry out compression test, specimens for each composition having dia 10mm, L/D =0.8 as per ASTM- E09 were compacted at an applied pressure of 700MPa. For 3-point bend tests the standard blocked specimen (31.5 x12.7 x 6.3 mm^3) as per ASTM B 925-08 were prepared at an compaction pressure of 480MPa. To minimize the effect of back stress developed during compaction each pellet were allowed for 2 minute holding time after every compaction.

Fig. 3.3 Cold uniaxial hydraulic press

Fig 3.4 High temperature tubular furnaces

3.3.4 Sintering

The green 15 mm diameter pellets obtained from cold uni-axial pressing were subjected to sintering in a tubular furnace in argon atmosphere (Purity 99.9%). The sintering temperature was varied from 850°C, 900°C and 1000°C maintaining the holding time constant as 1 hour at a heating rate of 5°/min The compression test samples and 3-point bend test samples were sintered at 900°C for 60 min and 90 min at a heating rate of 5°/min and 4°/min in the argon atmosphere. At the staring of each batch samples was placed inside the tubular furnace, initially the tube was evacuated to a vacuum level of 10^{-3} mbar pressure and Ar gas was purged through the tube in order to prevent the oxide formation at the surface during sintering and holding of the specimen. All samples were allowed to attain room temperature inside the tube of the furnace before exposing to the atmosphere.

3.3.5 Polishing

Each sample were polished through a sequence of emery paper of grade – 2, 3, 4. Samples were then polished using successively finer paper to 1200 grit followed by 1 and 0.3 μm alumina slurries. The fine disc polishing was done by coarse cloth polishing and fine cloth polishing. Diamond paste was used for the fine polishing.

3.4 Specimen characterization

3.4.1 X-Ray Diffraction

The polished samples were mounted on a grit slide. The phase evolution during different sintering temperature was characterized by X-Ray diffractometer. (PANalytical model: DY-1656, shown in Fig. 3.5). The diffraction patterns were recorded over a scan range of 20 – 80 ° at a step size of 2°/min using the CuKα (= 1.5418A°) radiation. The phases present at different sintering temperature and crystal structures of the product phases were identified from the peak positions(2Θ) values of the XRD pattern.

Fig. 3.5 Philips X-pert MPD X-ray diffractometer

3.4.2 Scanning electron microscopy (SEM)

Microstructural characterization of metallographically polished samples was carried out by scanning electron microscopy (JEOL 6480 LV, shown in Fig. 3.6). Ferric chloride solution (5 g $FeCl_3$ and 50 ml HCl in 100 ml distilled water) was used as an etchant to selectively attack the grain boundaries. Micrographs were taken at 20KV accelerating voltage. The morphology of the reinforcement particle, particle distribution, reinforcement particle-matrix integrity, matrix cavitations and grain size was observed from the SEM micrographs. The compositional analysis of a section was investigated by electron dispersive X-ray (EDX). The fractography study was also done by SEM to understand the modes of fracture, the failure of the interface, failure of the matrix, energy dispersive spectrometry) was done for the elemental analysis of a micrograph.

Fig. 3.6 JEOL JSM-6480LV scanning electron microscope

3.5 Physical property analysis

3.5.1 Density

The theoretical density of the each sample was calculated on the basis of rule of mixture.

$$\rho_{composite} = \rho_{Cu} \times vol\%\ of\ Cu + \rho_{Alumina} \times vol\%\ of\ alumina$$

The relative sintered density of the pellets was determined by Archimedes method. The polished samples were weighed in air, and when suspended in distilled water, using an electronic balance of least count of $\pm$0.001g. Contech CB series analytical balance (illustrated in Fig. 3.7) with a density measurement kit package from Contech was used for the density measurements.

Fig. 3.7 Contech CB series analytical balance with a density measurement kit

3.6 Mechanical Testing

3.6.1 Hardness

The samples were polished to a scratch free surface. Microhardness of the specimen was measured by Vickers hardness tester (Leco Microhardness Tester LM248AT, shown in Fig. 3.8) at an indenting load of 0.3kgf for a dwell time of 5 seconds. The readings were recorded here at four equivalent locations for each specimen.

Fig. 3.8 Leco Microhardness Tester LM248AT

Fig. 3.9 Ball-On-Plate Wear Tester TR-208 M1

3.6.2 Wear Test

In the present research work Ball-On-Plate Wear Tester TR-208 M1(Fig. 3.9) instrument was used to evaluate the wear behavior of the sintered composites. This experiment was done under a constant load of 10N for 10minutes at a speed of 30 rpm.

3.6.3 Compression test

The compression test was carried out in a universal testing machine (Instron- SATEC series servohydraulic machine, illustrate in Fig.3.11). A strain rate of 1mm/mm min^{-1} was maintained throughout the experiment. The stress – stain curve were estimated at a strain rate of $1sec^{-1}$. Each sample was reduced to the 50 % of their initial height. All samples are of cylindrical shape of dia 10mm and L/D = 0.8 (as per ASTM standard E9-89). Graphite powder with lubricating oil was used as lubricant in order to avoid the friction between the sample and anvil. The Hollomon analysis equation was used to determine the strain hardening exponent (n) from true stress and true strain values. $\sigma = k\varepsilon^n$

Where is the true stress value and being the true plastic strain, n is the strain hardening exponent.

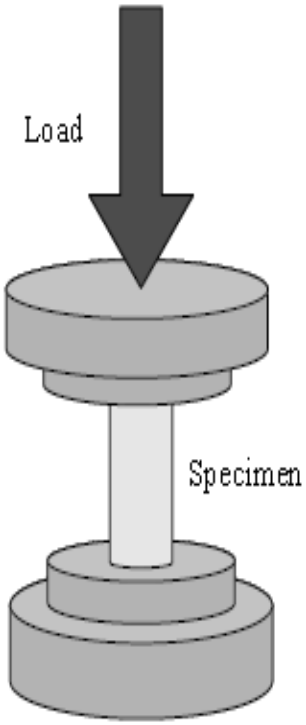

Fig. 3.10 Schematic diagram for the compression test

Fig. 3.11 Instron- SATEC series servohydraulic machine

3.6.4 3-point bend test

The 3-point bend test was carried out in an Universal testing machine(Instron- 5967, illustrate in Fig. 3.13) samples for transverse rupture test were prepared as per the ASTM B925. The width and thickness of the specimens were measured. A span length of 26mm and strain rate of 0.5sec^{-1} was maintained for the tests. The specimen was placed in the transverse rupture test fixture horizontally which is perpendicular to the supporting rod. A compressive force was applied parallel to the pressing direction. Transverse rupture strength (TRS) of the specimens was calculated from the following formula:

TRS $=(3 \times P \times L)/ (2 \times t^2 \times w)$

Where: TRS is the transverse rupture strength of the specimen in MPa, P is maximum load required to rupture the specimen (N), L represent span length or the center to center distance between supporting rods (mm) , w = Width of the specimen(mm) and t is thickness of the specimen(mm)

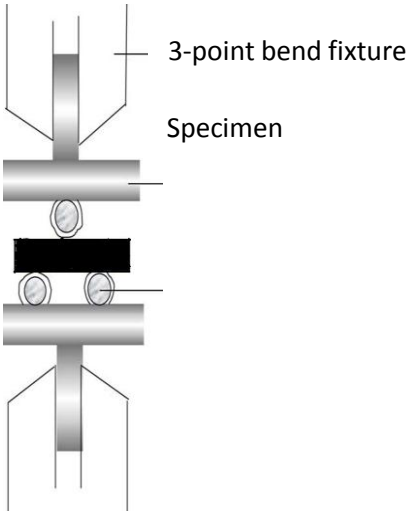

Fig.3.12 Schematic diagram for 3-point bend test

Fig. 3.13 Instron- 5967 servohydraulic machine

3.7 Thermal treatment

3.7.1Thermal shock

The 3-point bend test samples of Cu – 5% Al_2O_3 (10 micron) and Cu – 5% Al_2O_3 (< 50 nano) were chosen for thermal shock treatments. The three point bend test standard specimens were treated in a thermal shock environment with a 160°C temperature gradient by two separate

routes. For one batch of specimen it was from +80°C temperature to - 80°C temperature (down thermal shock) and for other batch it was in the reverse order (up thermal shock). The first batch of samples were exposed at +80°C isothermally for different period of time (1 hour, 15 minute) and immediately plunged into - 80°C temperature bath and exposed for same duration of time (1 hour, 15 minute). The second batch of samples was also treated for the same period of exposed time in the reverse temperature cycle. The third batch of samples was allowed to reach to 80°C continuously with furnace temperature and isothermal holding was done for 1 hour at that temperature. The same samples were transfer to the low temperature chamber and allowed to attain -80°C gradually and isothermal holding was done for 1 hour at that temperature. The fourth batch of samples was also treated for the same period of exposed time in the same heating profile as in batch 3 in a reverse temperature order. After each thermal treatment 3-point bend test of each sample was performed in Instron-5967 instantaneously to avoid any relaxation phenomenon of the composite at room temperature.

Fig. 3.14 Ultra low chamber

Fig. 3.15 Muffle furnace

3.7.2 Thermal conditioning

In order to treat the samples for thermal conditions the samples were categorized into 3 groups. The first group was treated at +80°C in muffle furnace (illustrate in Fig. 3.15) for 1 hour isothermally. The blower of the furnace was on function for heat circulation and uniform heating of the samples. Another set of samples were treated at -80°C in a ultra low temperature chamber(illustrate in Fig. 3.14) for 1 hour by isothermal holding. The third batch of samples was maintained at ambient temperature. 3-point bend test was done immediately at room temperature after each thermal conditioning.

3.7.3 Insitu high temperature 3-point flexural test

In same set of composition of samples in-situ 3-point bend test was carried out at a temperature of 250°C, 100°C. The samples were kept inside the furnace chamber. Furnace was allowed to reach the required temperature. As furnace had attained the required temperature the 3-point bend test was done instantly.

3.8 Fractrography

The fracture surface of the all 3-point bend test samples were investigated by scanning electron microscopy (JEOL 6480 LV). The fractography study revealed the various possible fracture mechanisms operating during the thermal shock, thermal conditioning, high temperature in-situ test and 3-point bend test at ambient temperature.

Chapter 4

Results and Discussions

4.1Phase analysis from X-Ray diffraction

4.1.1Micro-compositeX – Ray diffraction(XRD) pattern of Cu- Al_2O_3(p) micro composite sintered at 1000°C and 900°C are illustrated in Fig. 4.1(a)-(b). The X-ray peaks confirm the presence of Cu, Al_2O_3 and Cu_2O phases. The crystal structure of the copper is face centered cubic (FCC), Alumina is rhombohedral and Cu_2O is FCC crystal structure. With increases in vol. % of reinforcement the peak intensity of the Al_2O_3 peaks increase. As reinforcement content increases from 5% to 20% at a sintering temperature of 900° C the peak position of the pure Cu shift from 21.744° to 21.93°, as a result Cu lattice parameter decreases from 3.6A° to 3.57A° i.e. by 0.8%. As the volume faction of reinforcement increases the oxide peak intensity increases. At 1000° C the intensity of Cu_2O peaks is more likely to be prominent then less likely at 900°C sintering temperature this may be attributed by susceptibility of copper matrix to oxide formation at higher sintering temperature.

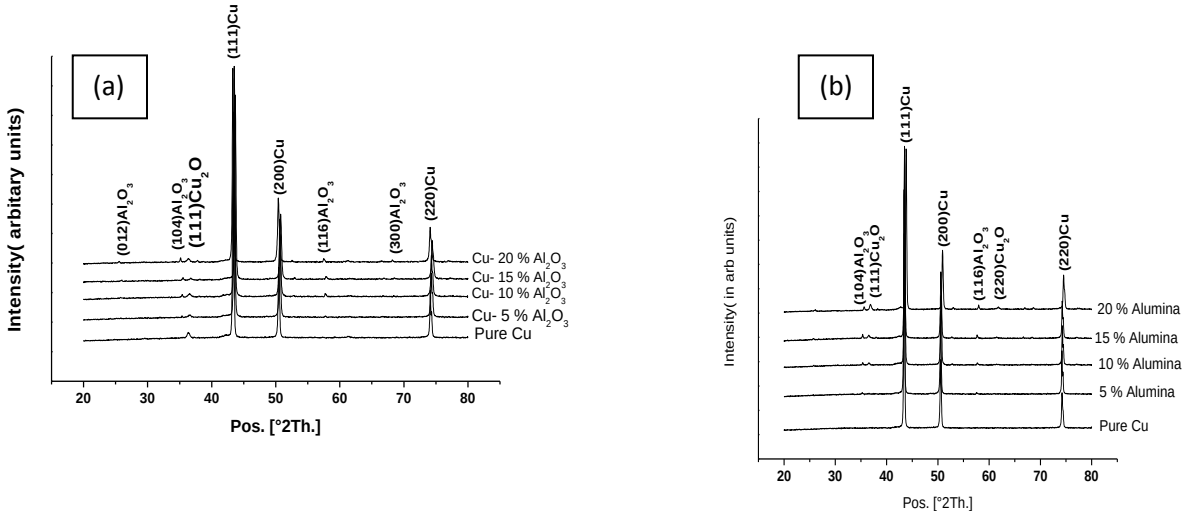

Fig. 4.1 XRD pattern of pure Cu, Cu- 5% Al_2O_3, Cu- 10% Al_2O_3, Cu- 15% Al_2O_3, Cu- 20% Al_2O_3 microcomposites sintered at (a) 1000° C and (b) 900° C.

4.1.2Nanocomposite

In Cu- Al_2O_3(p) nano-composite XRD analysis confirms the presence of Cu, Cu_2O, Al_2O_3 phases. As vol. % of reinforcement is very low it is difficult to identify the alumina peak. With increase in sintering temperature the oxides peak intensity decrease as Cu is more prone to oxide formation at higher sintering temperature. The Cu_2O peaks are more pounced in nanocomposite rather then micro composite. As nano particles are more prone to agglomeration this increases the clustering phenomenon with increase in Al_2O_3 content. Clustering leads to the generation of voids at the interface results in providing the new surface which exposes to oxide formation [52].

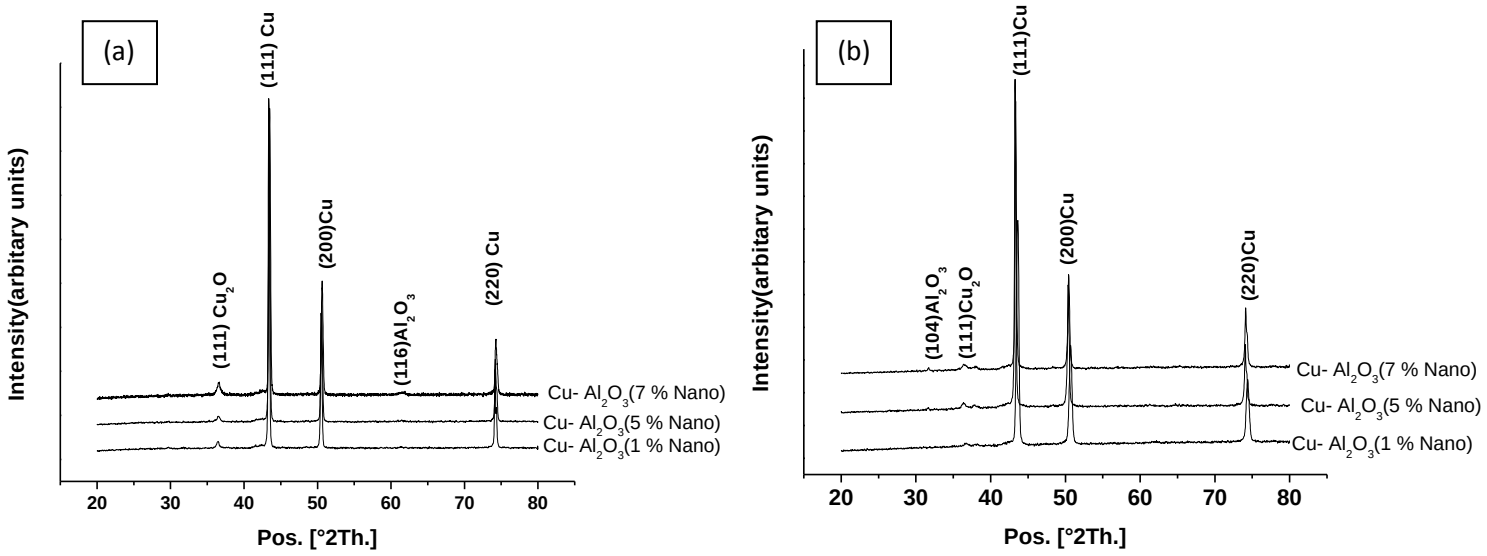

Fig. 4.2 XRD pattern of Cu- 1% Al_2O_3, Cu- 5% Al_2O_3, Cu- 7% Al_2O_3 nanocomposites sintered at (a) 1000° C and (b)900° C

4.2 Scanning electron microscopy

4.2.1 Microcomposite

The SEM micrographs give profuse information of reinforcement distribution, status of interface, clustering and mechanical phenomena like twinning. The black portion of SEM micrograph corresponds to the Al_2O_3 reinforced particle while the white region represent to the copper matrix scanned in back scattered electron mode. With raise in sintering temperature, reinforcement particle clustering decreases shown in Fig:4.3(a)-(c) This may be attributed by spreading of Al_2O_3 particles towards the copper particle boundaries due to the ductile nature of the copper[53].

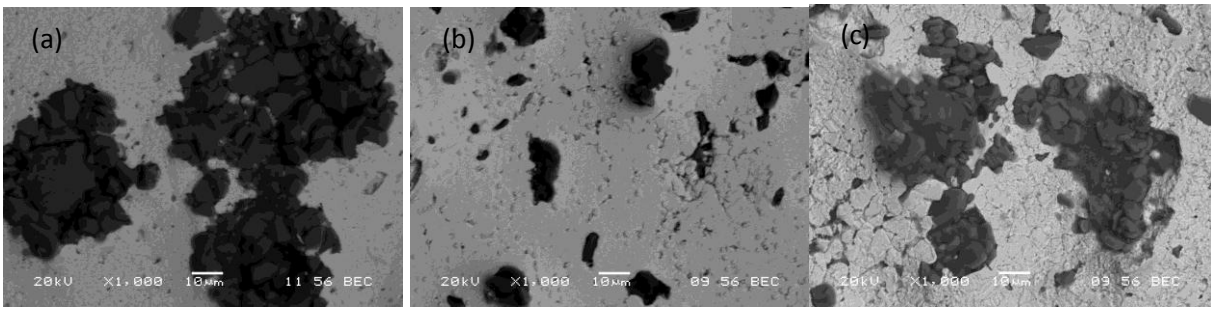

Fig. 4.3 SEM micrograph representing the reinforcement particle distribution of Cu – 5% Al_2O_3 microcomposites sintered at different sintering temperature(a)850°C, (b) 900°C and (c) 1000°C

Fig. 4.4(a)-(d) illustrates the spatial distribution of reinforcement in copper matrix with the increase in reinforcement content at a sintering temperature of 1000°C. With increase in volume fraction of Al_2O_3 probability of clustering also increases. This may be due to an inadequate ratio of the surface area of matrix particles to the reinforcement particles and density difference between the matrix and reinforcement which lead to the formation of cluster in high vol. % of the reinforcement [54]. Clustering can be minimized by maintaining the ratio of the particle size of the particulate to the particle size of the matrix approximately one [17,55].

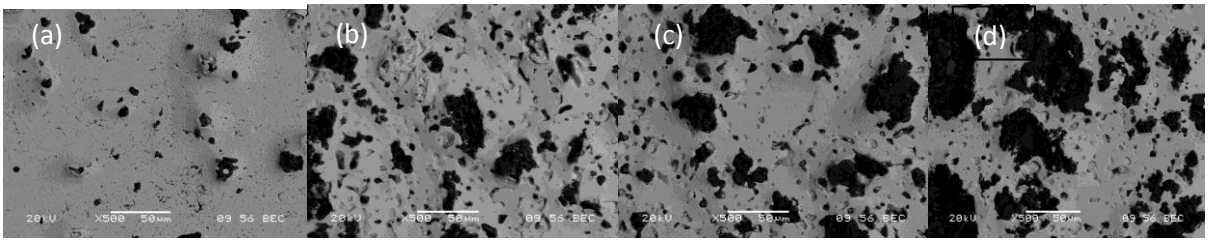

Fig: 4.4 SEM micrograph representing the reinforcement particle distribution of (a)Cu – 5% Al_2O_3,(b) Cu – 10 % Al_2O_3, (c)Cu – 15% Al_2O_3 and (d)Cu – 20% Al_2O_3 microcomposites sintered at 1000°C temperature.

Annealed twin bands has been more likely to found in Fig. 4.5 (a) of Cu-20% Al_2O_3 composite sintered at 900° C. on the contrary no twin band is seen in Fig. 4.5 (b) of Cu- 20% Al_2O_3 composite sintered at 1000° C. This may be due to the less no of active slip system (less then five) in 900°C sintering temperature and high stacking fault energy of the copper[3]. With increase in sintering temperature, the sessile dislocations which are generate during prior deformation process like powder blending and compaction may move by atomic diffusion or vacancies diffusion which is a temperature driven phenomenon.

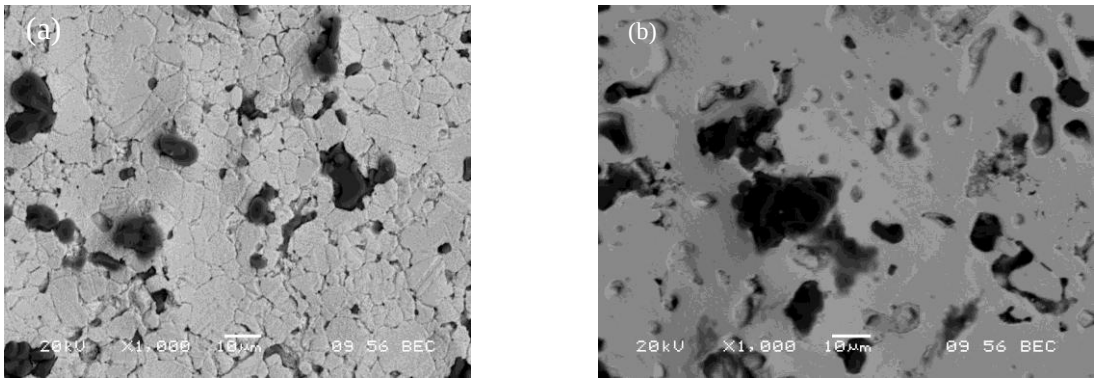

Fig: 4.5 SEM micrograph showing the presence and absence of annealed twin bands in Cu- 20% Al_2O_3 microcomposites sintered at (a) 900°C and (b) 1000°C.

Interface de-cohesion and particle cracking which are the premature failure phenomenon of the metal matrix composite are observed in Fig. 4.6(a)-(c) Maximum stress generate in the matrix is

at the pole of the particle as the sharp corner of the reinforced particle act as a stress raiser point. [53,56]. The stress concentration near the particle leads to the development of high local strain relative to the applied global strain. Peak stress component of the particle increases with increases in the volume fraction of reinforcement making the particles more susceptible to particle cracking. Clustered regions act as a nucleation site for damage initiation and further propagation of fracture by linking the damage of clustered region cause composite weakening.

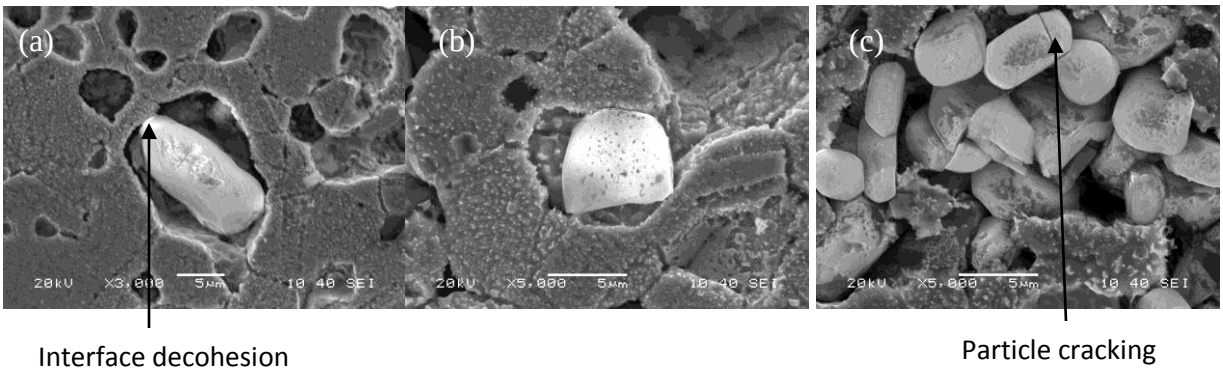

Fig. 4.6 SEM micrograph illustrating the premature damage in the microcomposite (a)–(b) the pole of the particle is the nucleation site for interface decohesion and (c) particle cracking in the clustered region

4.2.2 Nanocomposite

The SEM micrographs of copper-alumina nanocomposites illustrate improved distribution of alumina in the matrix compared to that in microcomposites.

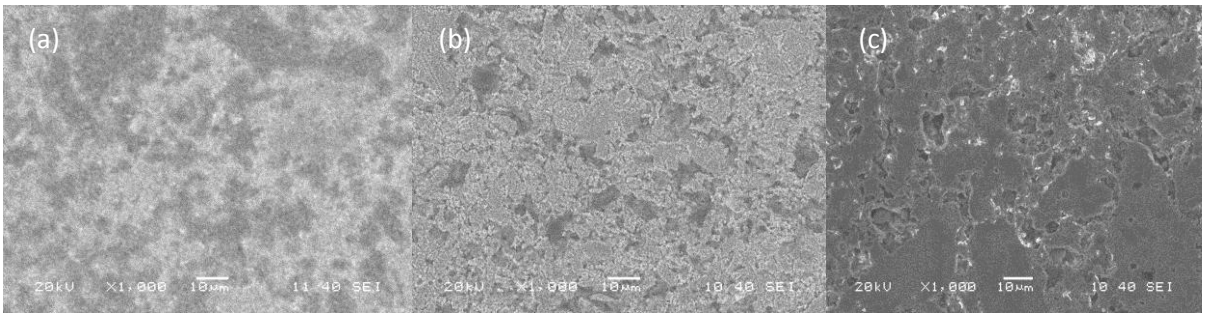

Fig. 4.7 SEM micrograph representing the reinforcement particle distribution of Cu – 5% Al_2O_3 nanocomposites sintered at different sintering temperature (a) 850°C, (b) 900°C and (c) 1000°C

The agglomeration of alumina nanoparticles is quite vigilant in the Fig. 4.7(a). The pinning effect of nano particle are more likely to be pronounced at 900°C sintering temperature which is evident from Fig. 4.7(b). The SEM micrograph of Fig. 4.7(c) revels that nanocomposite sintered at 1000°C have larger grain size indicating that grain growth occur at higher sintering temperature.

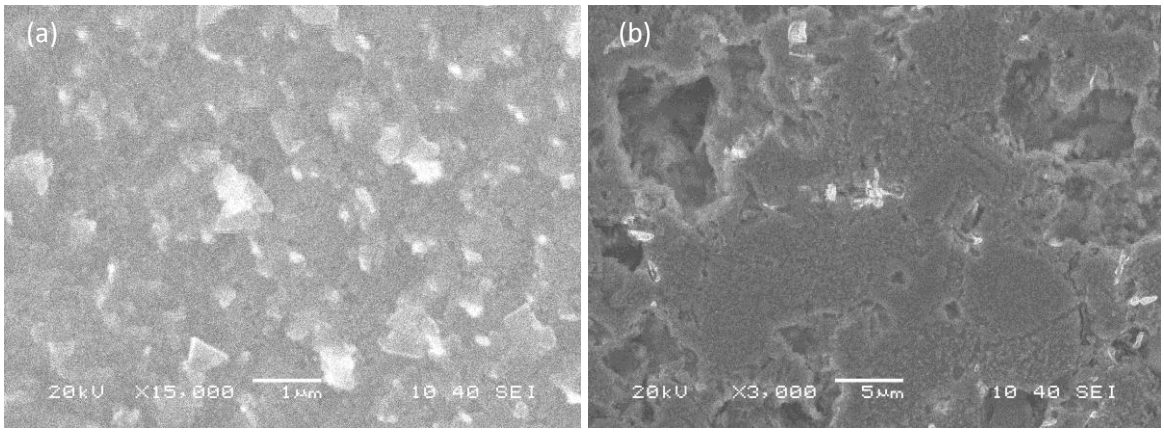

Fig. 4.8 SEM micrograph representing the matrix-reinforcement compatibility in Cu – 3% Al_2O_3 nanocomposites sintered at different sintering temperature (a) 900°C and (b) 1000°C

The embedment of alumina nanoparticles in copper matrix is appreciably deeper than in the microcomposites illustrated in Fig 4.8(b). The enhanced physical contact of alumina nanoparticles with the matrix can be attributed to the high atomic diffusivity of the nanoparticles. The stabilization of the surface energy of nanoparticles is a thermodynamic driven phenomenon; hence it is quite obvious that the physical intimacy is better in nanocomposites.

4.3 Density

Density measurements were carried out using the Archimedes method and the theoretical density was calculated from the rule of mixtures. Fig. 4.9(a)-(b) represent the densification of Cu –Al_2O_3 micro-composites and nano-composite with increase in vol. % of reinforcement content at various sintering temperatures.

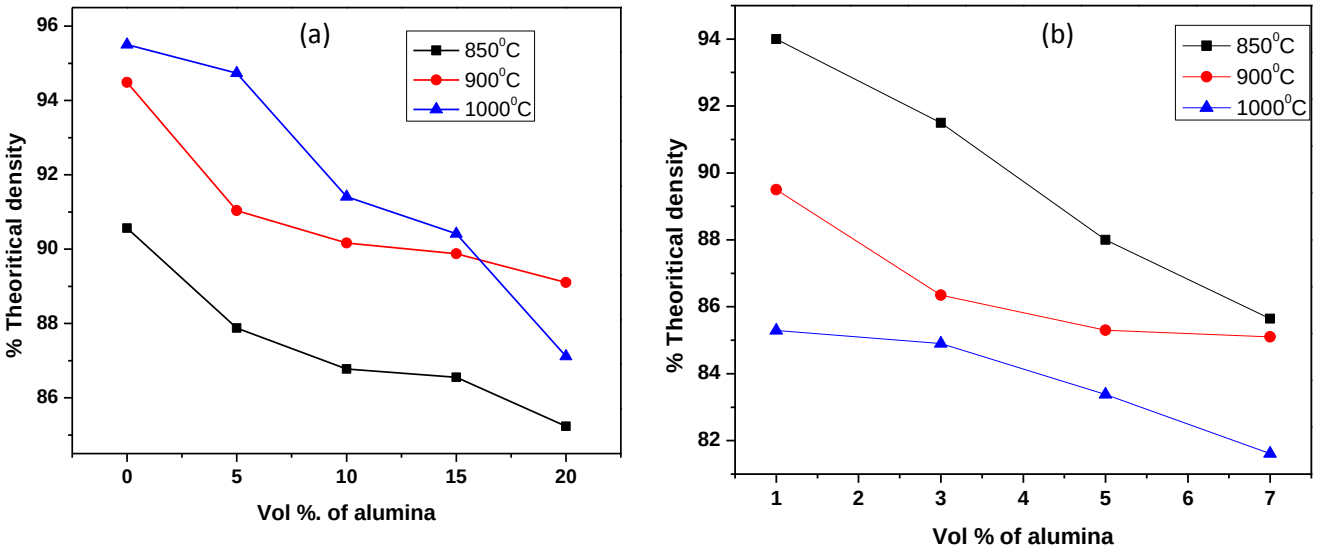

Fig: 4.9 Densification plot of (a) micro-composites and (b) nanocomposites with different vol. % of Al_2O_3 sintered at different sintering temperature.

From the Fig: 4.9 (a)-(b) it was found that amount of densification decreases with increase in vol.% of reinforcement content. This may be due to lower density value of Al_2O_3 particles(3.95gm/cm^3) than that of pure copper(8.9gm/cm^3) [53]. The detrimental phenomenon like particle fracture, interface de-cohesion, matrix void are more likely to present in high vol. % of reinforcement(evident from the SEM micrographs Fig. 4.6) decreases the densification of the composite[57]. The creation of voids in the matrix hinders the densification and impedes the continuity in interface compatibility of copper and alumina [53].

4.3.1 Microcomposite

In case of microcomposite the increase in densification at a temperature of 1000^{o}C as compared to the 900^{o}C sintering temperature may be attributed by partial melting of the matrix and enhanced cementing phenomena. Matrix grain growth occurs at higher sintering temperature which decreases the pore content in the micro composite leading to the higher densification value at 1000°C. For 20 Vol. % of reinforcement content % of theoretical density decreases from 89.10% to 87.16% with increase in sintering temperature from 900°C to 1000°C.

4.3.2 Nanocomposite

In case of nano-composite as the interfacial area is more, the detrimental effect of interfacial phenomenon are more likely to prevail at high sintering temperature and less likely at lower sintering temperature. The maximum density value was observed for the sintering temperature at 850°C. As the nano-particles are more likely to agglomerate, sintered density decreases with increase in the reinforcement content providing new surface exposed for oxide formation[52]. The increases in sintering temperature also have a detrimental effect on density of the nanocomposites. enhanced formation of Cu_2O (Fig. 4.2) representing that the matrix is more susceptible to oxide formation at higher sintering temperature which leads to void formation at the matrix and at the interface.

4.4. Microhardness

The mean micro-hardness value was determined by taking the average of five closely spaced values. Fig: 4.10(a) represents the microhardness values (HV) of Pure Cu and Cu–Al_2O_3 micro-composite with a variation of reinforcement content. Fig. 4.10 (b) the micro-hardness values of

Cu-Al_2O_3 nanocomposite with a variation in vol. % of reinforcement content at different sintering temperature. The hardness value of pure copper is 49.5 HV. (Goodfellow, 1993/94).The hardness (HV) of the composites increases with increase in reinforcement content in the matrix.

This may be attributed by the inherent property of hard alumina reinforced particle.

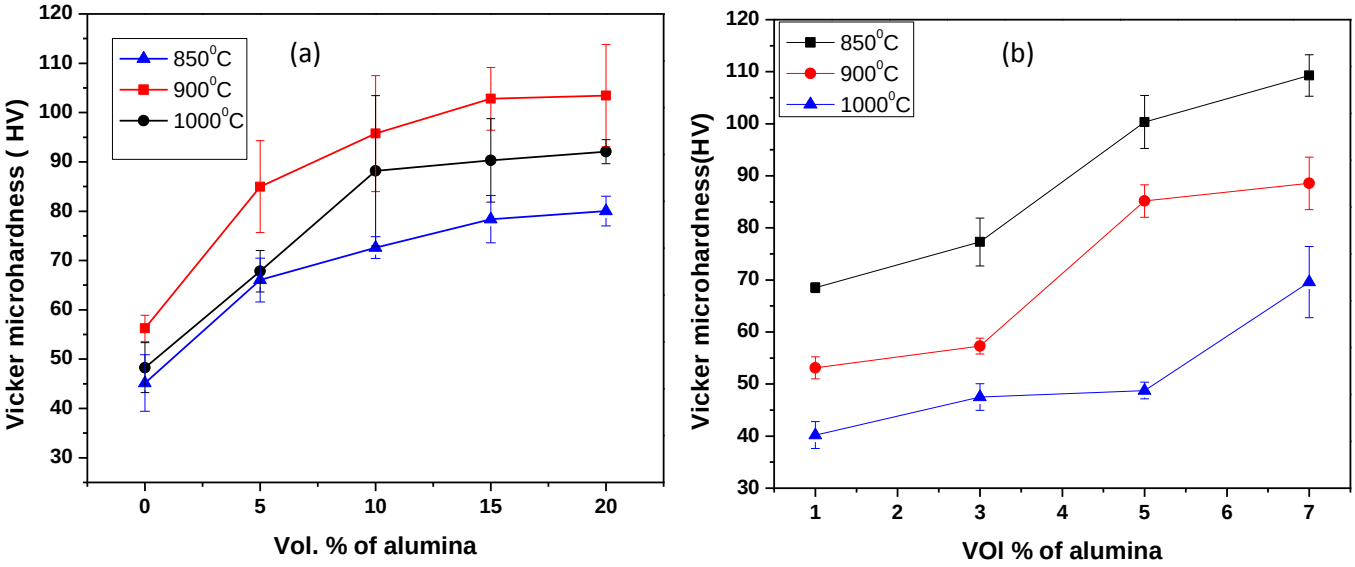

Fig: 4.10 Microhardness plot of (a) micro-composites and (b) nanocomposites with different vol. % of Al_2O_3 sintered at different sintering temperature.

4.4.1Microcomposite

In case of micro-composite micro-hardness values first increases with increase in sintering temperature from 850°C to 900°C but further increase in sintering temperature to 1000°C hardness values decreases which may be attributed to the grain coarsening of matrix [53,58] at higher sintering temperature. This can be attributed to improper contact between the reinforcement and matrix due to thermal stress relaxation at the interface imparted by high

processing temperature i.e. 1000°C. Microcomposites sintered at 900°C have the highest hardness value as compared to the composites sintered at 850°C and 1000°C. Hence the 850°C can be considered as the under-sintering and 1000°C as the over-sintering temperature for copper-alumina microcomposites.

4.4.2Nanocomposite

In case of nano composite nano alumina has high hardness which impedes the movement of dislocation during plastic deformation. Nano-alumina restricts the grain growth of the copper matrix and results in grain refinement of copper matrix. The hardness of the composite gets improved with increase in the reinforcement content. With increase in sintering temperature the surface activity gets predominant. The hardness values are maximum for the composites sintered at 850°C temperature. This can be further explained as the density of the composite are higher at 850°C. The alumina nanoparticles tend to cluster which decreases the Orowan strengthening effect. The hardness values trend represents the better sinterability of copper-alumina nanocomposites at low temperature such as 850°C. The highest hardness values recorded are 108 HV for 7 vol. % reinforced copper-alumina nanocomposites. The density hierarchy complements the hardness trends followed at different sintering temperatures. The lowest sintering temperature imparts highest density to the nanocomposites, and this trend is also followed by rest of the temperatures. This can be ascribed to the fact that the interface dimension in the nanocomposites is high, leading to increased susceptibility to interfacial decohession.

4.5Wear

The abrasive wear rate is greatly reduced as Al_2O_3 content in the composite increases. However, as the number of fine Al_2O_3 particles increase, the resistance to the penetration of abrasive particles increases (Hardness increases with increases in the reinforcement content) and hence the depth of penetration by the ball is reduced leading to better abrasive wear resistance [59]. The drastic reduction in wear rate may be attributed by (1) enhancement in hardness of the composite reinforced by Al_2O_3 particles. [60] and (2) Large reduction of direct load contact between the Cu/Al_2O_3 composite interface and disk in comparison with pure copper as due to inherent property of hard Al_2O_3 particles.

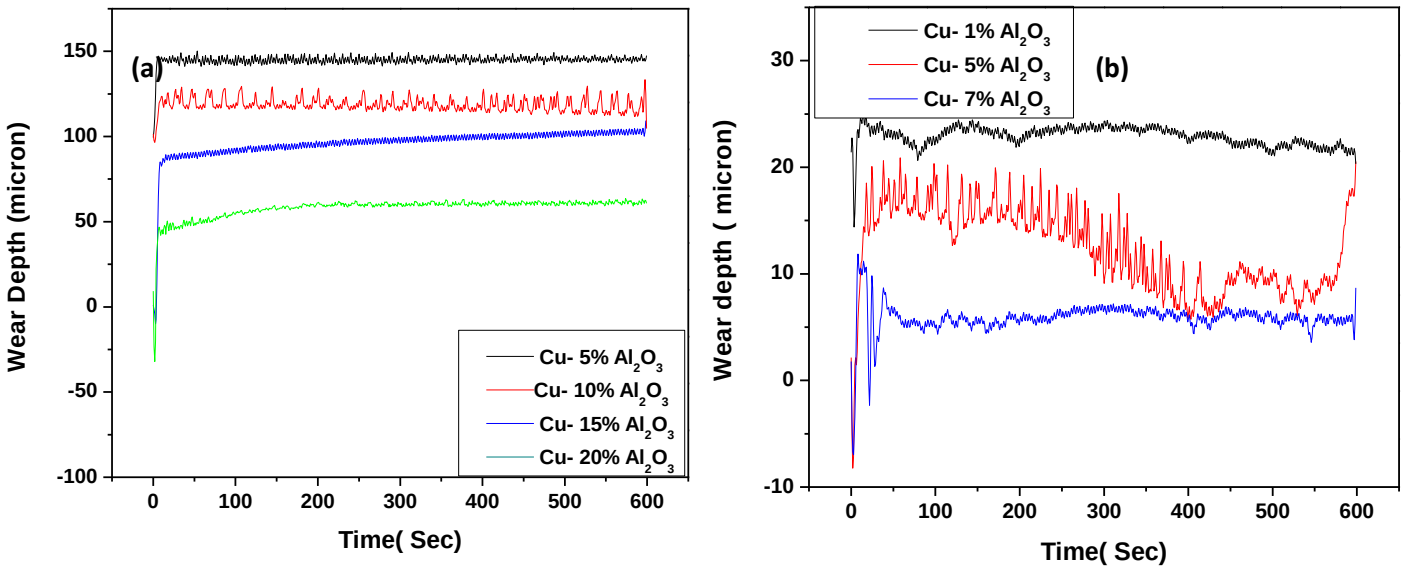

Fig: 4.11 Plot for wear depth verses time (a) micro-composites and (b) nanocomposites with different vol. % of Al_2O_3 sintered at 850°C temperature.

Fractography analysis of wear surface

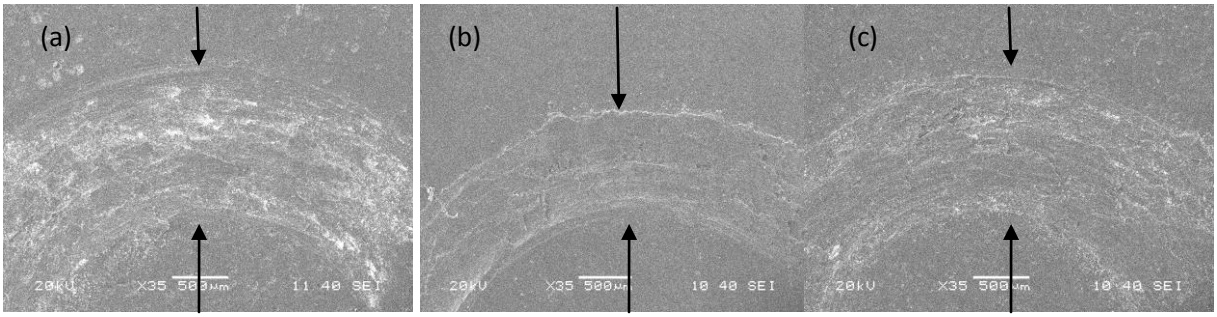

Fig: 4.12 SEM images of worned out surfaces of (a) Cu-5 vol. %Al_2O_3(micro) (b) Cu-10 vol. %Al_2O_3(micro) (c) Cu-1 vol. %Al_2O_3(nano)

From the SEM micrographs (Fig: 4.12) it has been observed that the wear track width increses as per the following trend:

Cu-10 vol. %Al_2O_3(micro) <Cu-1 vol. %Al_2O_3(nano) <Cu-5 vol. %Al_2O_3(micro). The Fig.4.12 represents narrow wear track in nanocomposites than in the microcomposites.

The SEM micrograph represents that with increase in reinforcement content the surface roughness decreases.

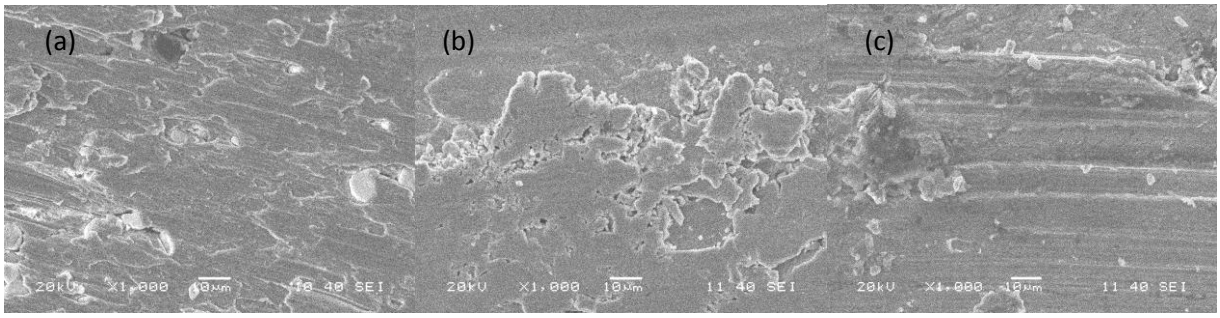

Fig: 4.13 SEM micrograph of wear surface of Cu –Al_2O_3 nanocomposite wth (a) 1% reinforcement, (b)-(c) 5% reinforcement.

As nano particles act as obstacle for the smooth removal of material the abrasion resistance increases with increses in the reinforcement content. In case of pure copper adhesive wear is the prevalent phenomena with extensive plastic deformation, where as alumina reinforced particle

has undergone abrasive wear. There are smooth and irregular areas are present in the micrograph in Fig.4.13(a). The smooth areas are may be due to the polishing effect at the start of the wear test. Worn surface of Cu- 5% Al_2O_3 nano composite(shown in Fig. 4.13(b)) reviles microgrooves are present on the worn out surface which is the result of ploughing action of the wear debris. The wear mechanisms operative at 20N of load are plastic ploughing and grooving of cu matrix. The worn surfaces of the composites can be characterised by long grooves(illustrated in Fig.4.13(c)) which results from micro ploughing across the surface and material removal into the ridges of the groove. The intensity of micro ploughing is substantially less on the composites containing higher amount of alumina.

4.6 Compression

4.6.1Microcomposite

The compressive stress-strain curves of microcomposites are illustrated in Fig: 4.14. The true stress–true strain value decreases with increase in reinforcement content. The mismatch of thermal conductivity between the copper matrix (401 k - W/(m.K)) and reinforced alumina particle (30 k - W/(m.K)) leads to the localized rise in temperature in a narrow range. Local temperature rise has no effect on reinforcement particles, while it can lead to the softening of the matrix locally, some region even be melted. As a result flow stress decreases. With increase in reinforcement content hardness values also increases which is the resistance to plastic deformation. So the compressive strength decreases.

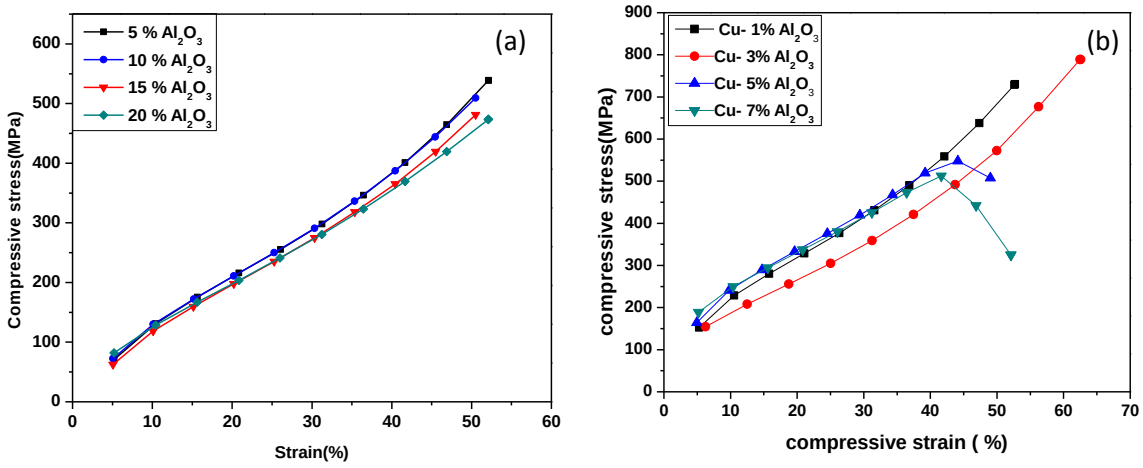

Fig: 4.14 True stress- true strain compressive plot for (a) Microcomposite, (b) Nanocomposite.

4.6.2Nanocomposite

The results from stress- strain curve of Cu- Al_2O_3 nanoparticle (Fig. 4.14(b)) shows that dispersions of nanoparticle have pronounced effect in enhancing the compressive strength with increases in reinforcement content. The noteworthy increase in compressive strength of alumina reinforced copper composite from a copper matrix could be attributed to : (i) significant grain refinement, (ii) the presence of reasonably distributed harder particulate, (iii) strengthening arises from increase in dislocation density of the matrix because of different thermal expansion coefficients of the matrix and particles [60], (iv) direct load transfer from matrix to reinforcement [61] and (v) Orowan strengthening mechanism [62]. The compressive stress decreases for further increase in reinforcement content. This may be attributed to void formation by interface decohession at the clustered regions as nano particles are more tends to agglomerate.

4.6.3 Calculation based on compression data

The strain-hardening exponent (n) was calculated from the true stress-strain curves. For elastically deformed composite the strain hardening exponent n can be estimated as:

{where, n = (ln $_1$/ $_2$)/ (ln $_1$/ $_2$)}

The composite reinforced with micro particle tends to fail through particle fracture which leads to decrease in strain hardening exponent. With increases in reinforcement content composite tends to fail through void nucleation, growth, and coalescence in the matrix regions near particles. The above failure mechanisms lead to the decrease in strain hardening exponent. The variation of strain hardening exponent with vol. % of reinforcement content is illustrated in Fig 4.15(a).

For nanocomposites, the presence of particles induces an inhomogeneous elastic strain due to the elastic modulus mismatch between the copper matrix (117 GPa) and reinforced alumina particle(300 Gpa). The elastic strain leads to the generation of high geometrically necessary dislocation density ρ_G in the composite matrix interface. The increased geometrically necessary dislocation density ρ_G leads to a higher work hardening in the matrix, thus leads to a higher composite flow stress. With increase in volume fraction of the reinforcement content clustering of nanoparticle increases. It increases the inter particle distance between the nano particles which subsequently reduce the particle dislocation interaction and also less strength is required to move a dislocation with larger inter-particle distance. This cause composite weakening which leads to decrease in strain hardening exponent with increases in the reinforcement content(illustrated in Fig: 4.15(b).

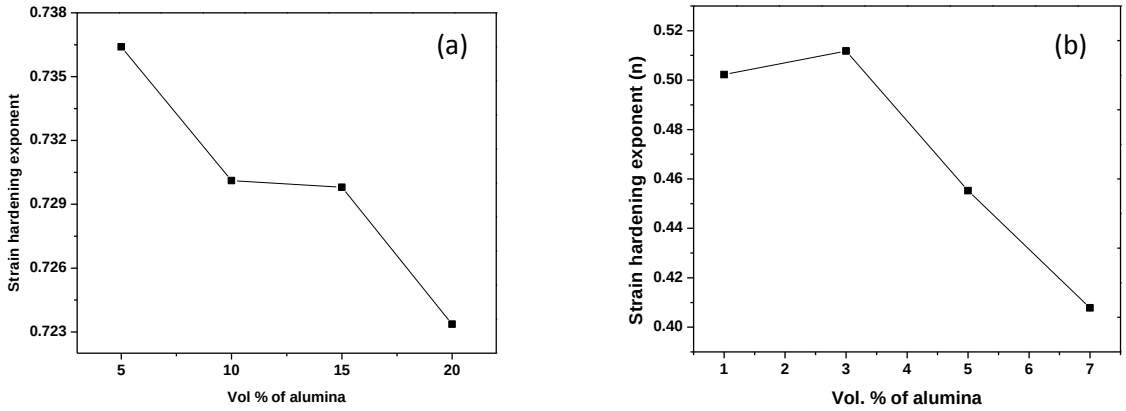

Fig: 4.15 Strain hardening exponent verses vol. % of reinforcement content plot for (a) Microcomposite, (b) Nanocomposite

4.6.4 Fractography of compression samples

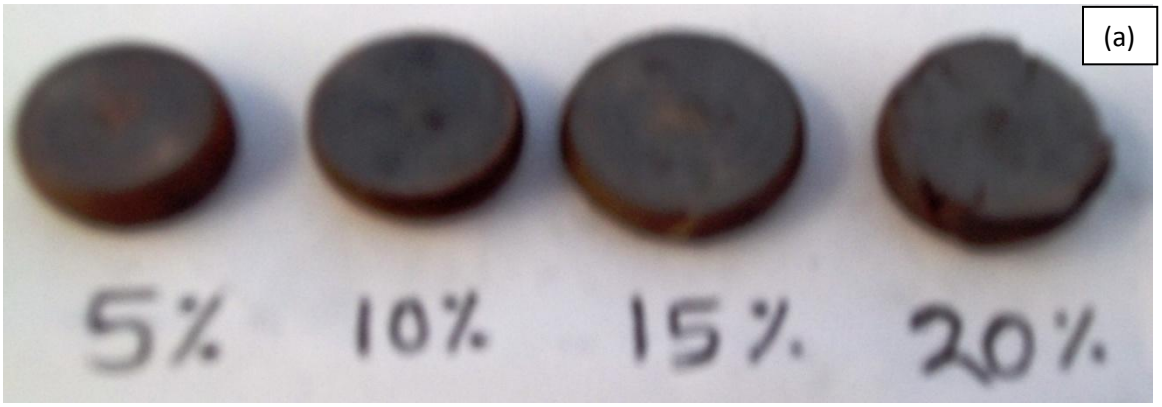

Fig: 4.16(a) Fracture surface of compression samples of microcomposites

The fractographs of different deformed microcomposites and nanocomposite at room temperature for initial strain rate of 1 min^{-1} are shown in Fig. 4.16. It's observed that the shape of compression specimens gradually changed their original shapes from cylinder to barrel-like shape during the deformation due to friction between the surfaces of the specimens and graphite plates. In case of micro composite the crack in the samples are 45° to the applied load axis(illustrate in Fig. 4.16(a)). This is indicates that shear mode of fracture is the dominant failure mode during compression.

Fig: 4.16(b) Fracture surface of compression samples of nanoocomposites

In case of nanocomposite it was observed during the compression tests that, all tested nanocomposite specimens were cracked before reaching 50% reduction in height. There is no specific angle at which the crack propagates (illustrate in Fig. 4.16(b)). It is observed that increasing Al_2O_3 content composites are more prone to circumferential cracks.

4.7 3-Point bend test

From the 3-point bend test result it was found that ultimate flexural strength value decreases with increase in volume fraction of the reinforcement content for both microcomposite and nanocomposite which is illustrated in Fig. 4.17(a)-(b).

4.7.1 Microcomposite

In case of microcomposites particle cracking is the most prevellent phenomena observed from SEM micrograph (Fig. 4.6(c)). According to Griffith criterion cracked particle in the clustered region prevents dislocation pile up which decreases the particle strengthening effect results in decreases in ultimate flexural strength value. The another reason for decrease in composite flexural strength with increase in alumina content may be due to the increase in degree of damage accumulation with increase in reinforcement content. Early fracture possibly occurs by linking the damage in clustered regions as a result ultimate flexural strength value decreases. The

decrease in strength of the composite leads to the decrease in toughness of the composite. Fig. 4.17 reveals a marginal increase in flexural modulus of the composite with an increase in reinforcement content.

4.7.2 Nanocomposite

In case of nanocomposite the ultimate flexural stress is appreciably high, rendering the commendation to alumina nanoparticles in copper matrix. As nano particles are more seems to agglomerate this decreases the interparticle distance(λ). The stress required for a dislocation to pass a reinforcement (τ_0) is indirectly proportional to the interparticle distance (λ) by the following relationship.

$$\tau_0 = \frac{Gb}{\lambda}$$

As interparticle distance increases easy movement of dislocations likely to be possible which restricts the dislocation pile up leading to composite weakening.

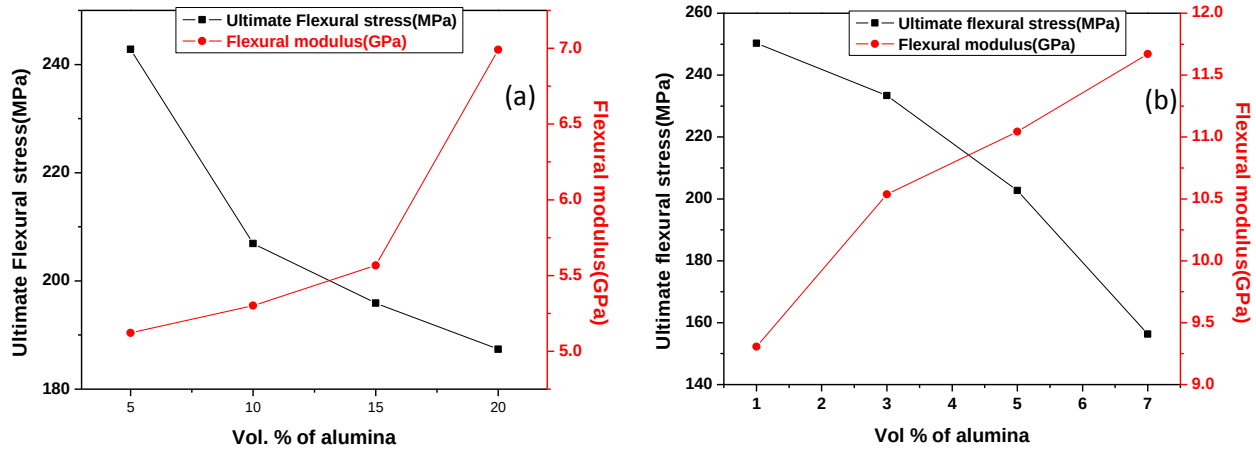

Fig: 4.17 Plot for ultimate flexural stress (MPa) and flexural modulus (GPa) verses vol % of reinforcement content for (a) microcomposites (b) nanocomposites

4.7.3 Fractography of 3-point bend test samples

Fracture surface of the 3-point flexural test microcomposites are shown in Fig. 4.18(a) - (c). The dimple fracture surface confirms ductile fracture as the principal mode of fracture in the

composite. Fracture surface of the composite exhibit micro-void coalescence in the matrix and particle cracking or de-cohesion. No secondary cracks are observed in the brittle Al_2O_3 particle indicating premature failure of the composite. Damage is nucleated by interfacial de-cohesion (Fig. 4.18(a)), particle cracking, void growth and finally coalescence of void. The dimple size decreases and number of dimples increases with increase in the reinforcement content. This could possibly be attributed to the energy required for plastic deformation of the matrix is predominantly absorbed than the energy required for crack tip to create new crack surface. The sharp micro-cracks that develop due to particle fracture can enhance localized plastic flow within the ductile matrix leading to matrix cracking (Fig. 4.18(c)) which aids in failure phenomena such as ductile separation of the matrix by void growth and shear bands. For high volume fraction of reinforcement contents, early fracture of materials occurs with minimal plastic deformation. The peak strain value decreases with increase in reinforcement content signifying the strain hardening behavior of the composite increases with increase in the reinforcement content. Defects such as porosity, macro microcracks and interface de-registry promote premature failure and ultimate fracture occurs earlier.

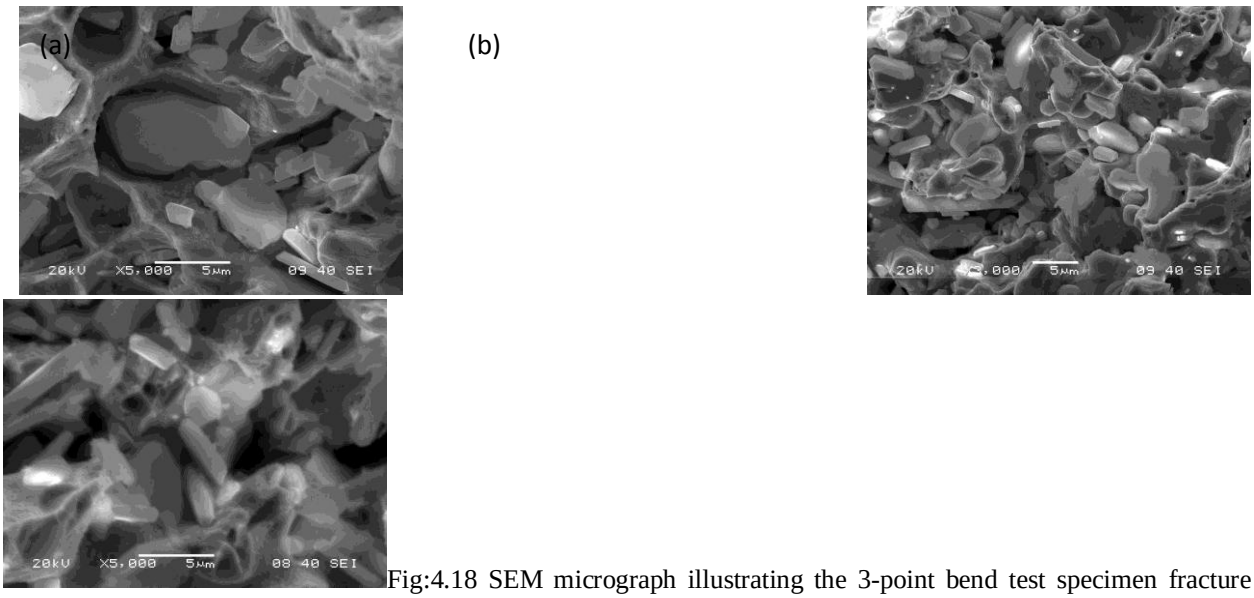

Fig:4.18 SEM micrograph illustrating the 3-point bend test specimen fracture surface of microcomposite having composition (a) Cu- 5% Al_2O_3, (b) Cu- 10% Al_2O_3, (c)Cu- 20% Al_2O_3

The fractography results of nanocomposite revels that the fracture mode is mainly dominant by brittle fracture. This can be attributed to the presence of nano alumina particle which restrict the plastic deformation of the ductile matrix. The macroscopic features of Cu-Al_2O_3 nanocomposites fracture surface indicate flat surface, minimal plastic deformation preceding the fracture and rapid crack growth accompanied by loud noise [30]. The microscopic characteristics includes faceted and transgranular fracture surface (Fig.4.19(a)), matrix cracking (Fig.4.19(b)) and river lines(Fig.4.19(c))

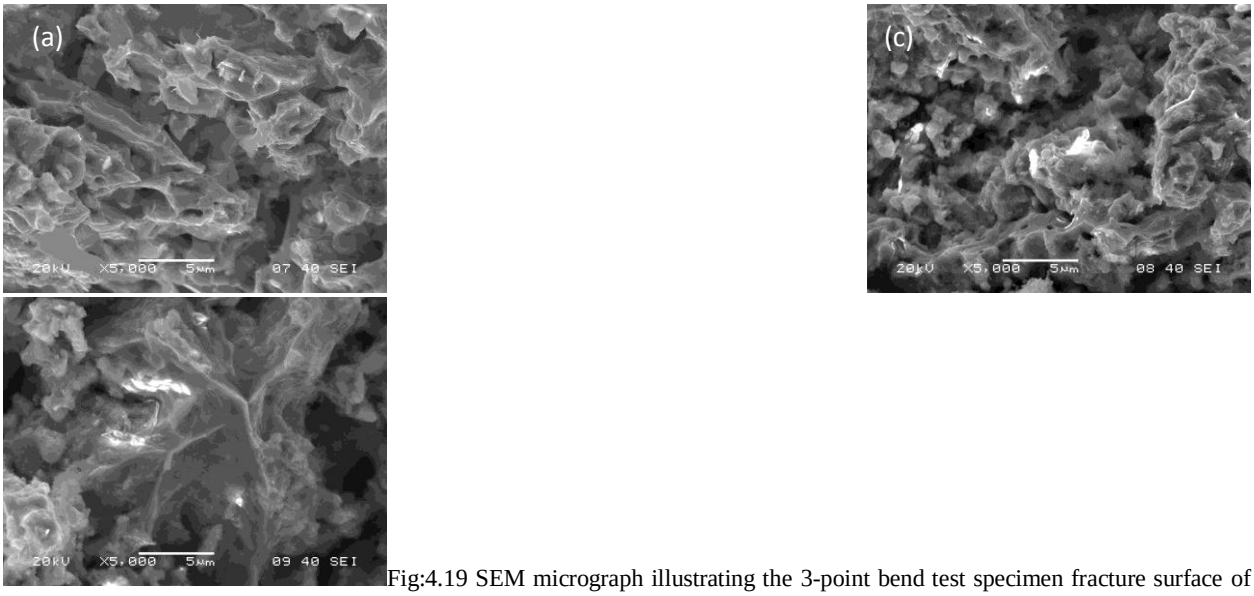

Fig:4.19 SEM micrograph illustrating the 3-point bend test specimen fracture surface of nanocomposie having composition (a) Cu- 1% Al_2O_3, (b) Cu- 5% Al_2O_3, (c) Cu- 7% Al_2O_3

4.8 Thermal shock

The thermal shock resistance has been estimated from the 3-point bend test samples. Fig; represent the ultimate flexural strength of the composite under various thermal shock exposures. The specimens were subjected to up-thermal shock (treated at -80°C followed by +80°C) and down-thermal shock (treated at +80°C followed by -80°C) for various exposure time.

Treatment Module	Treatment type
Module 1	Samples were kept in side the furnace/ low chamber. Then the instrument was allowed to reach at the desire temerature, isothermal holding of the samples for 1 hour at the desire temperature.
Module 2	The samples were kept inside the furnace/ low chamber for 1 hour after it reach the desired temperature
Module 3	The samples were kept inside the furnace/ low chamber for 15 minutes after it reach the desired temperature

4.8.1 Microcomposite

The ultimate flexural strength of microcomposites increases in both up-thermal shock treatment and also down-thermal shock treatments. There is an increment of 21.95% in flexural strength value for the up-thermal shock treatment in module-1, whereas down-thermal shock treatment increases the bending strength value by 29.69%. The mismatch of thermal coefficient of expansion of the copper matrix and alumina reinforced particle generate the geometrically necessary dislocation around the reinforced particles. When the sample is suddenly cooled to the ultra low temperature of -80°C, the generated dislocations are punched in the copper matrix in the vicinity of alumina particles. This develops a residual stress or back stress on the composite. The generated back stress resists the plastic flow of the matrix with the aid of reinforced particle which leads to the composite strengthening [23]. At +80°C the matrix expand and it imparts a compressive force on the particle. This leads to increase in interfacial integrity and also an evidence of particle fragmentation has been observed (evident from fig.4.22(b)). When the same specimen is treated at ultra low temperature i.e. -80◦C the matrix contracts eventually. This leads to the particle partial pull-out of the matrix-particle interface (evident from fig.4.22(c)). The increase in strength in both up and down-thermal shock treatment can be ascribed to the predominance by the former or starting treatment effect. The subsequent treatment is not able to reverse the initial effect on the same scale and degree.

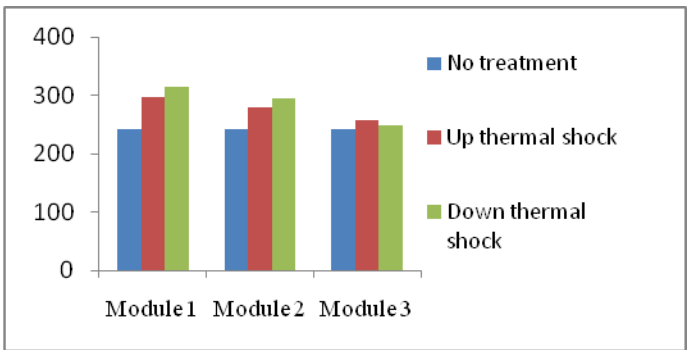

Fig. 4.20 Comparission of ultimate flexural stress (MPa) value for up-thermal shock and down-thermal shock of microcomposite treated in different treatment module

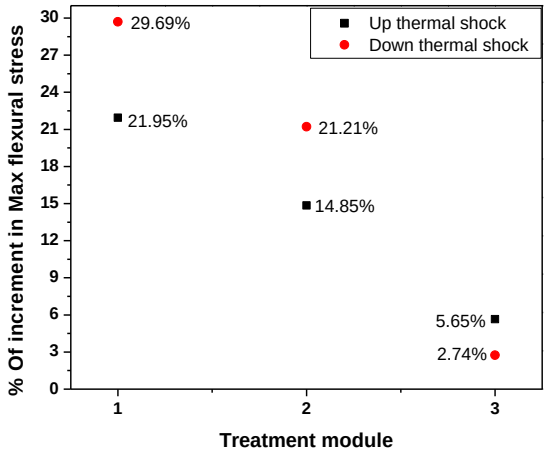

Fig. 4.21 % of increment in ultimate flexural stress (MPa) value for up-thermal shock and down-thermal shock with respect to no treatment of microcomposite treated in different treatment module

Fractography of the thermal shock treated microcomposite

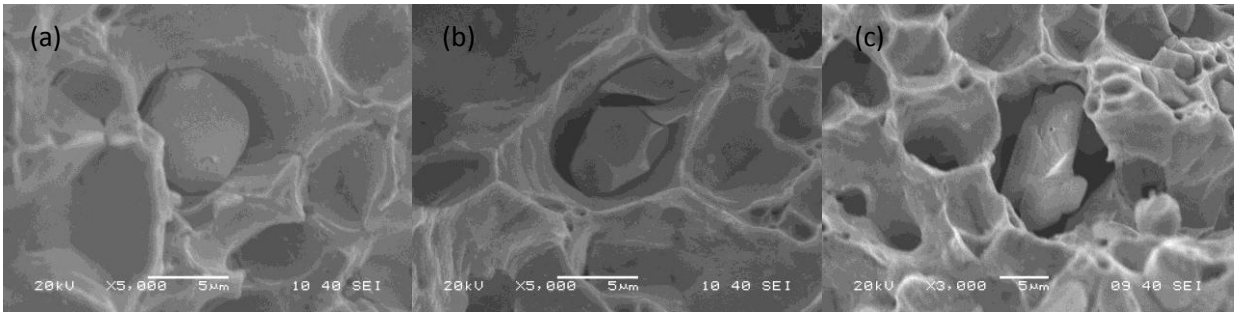

Fig:4.22 SEM micrograph illustrating the thermal shocked 3-point bend test specimen fracture surface of microcomposites (a)no treatment (b) down-thermal shock (c) up-thermal shock

4.8.2 Nanocomposite

In case of nanocomposite, the ultimate flexural strength value decreases for up-thermal shock whereas the strength values increases for down-thermal shock. In case of up-thermal shock the matrix in the vicinity of the particle contracts at -80°C temperature. This leads to the interfacial deregistry, the surface area of the nano particles being higher the degree of deunion is also high rendering the interface weak. The above being a physical phenomenon cannot be reversed/

restored at +80°C temperature, hence the ultimate flexural strength decreases. The effect of primitive treatment is predominant over the succeeding treatment. In case of down-thermal shock, the degree of physical contact of matrix and the reinforced nanoparticle increases at +80°C temperature. The ultimate flexural strength increases for being the high surface area of nanoparticles which resulting in the increase of the improved interfacial area. Hence the exposure at -80°C temperature could not induce damage on the same scale.

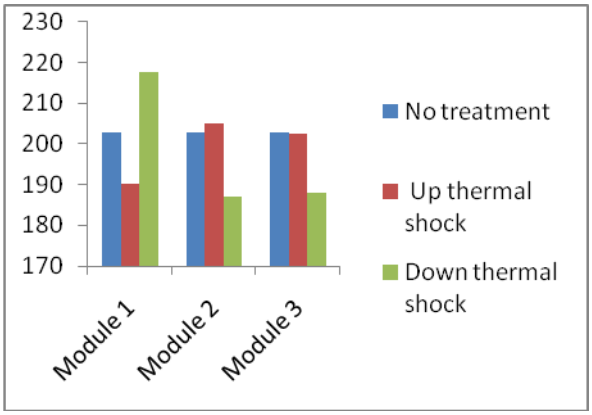

Fig. 4.23 Comparission of ultimate flexural stress (MPa) value for up-thermal shock and down-thermal shock of nanocomposite treated in different treatment module

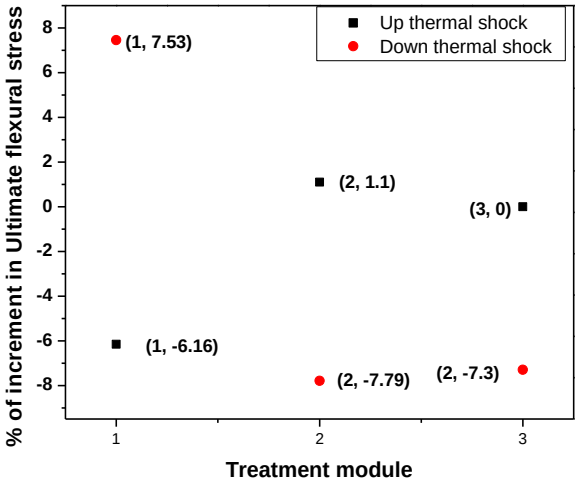

Fig. 4.24 % of increment in ultimate flexural stress (MPa) value for up-thermal shock and down-thermal shock with respect to no treatment of nanocomposite treated in different treatment module

Fractography of the thermal shock treated nanocomposite

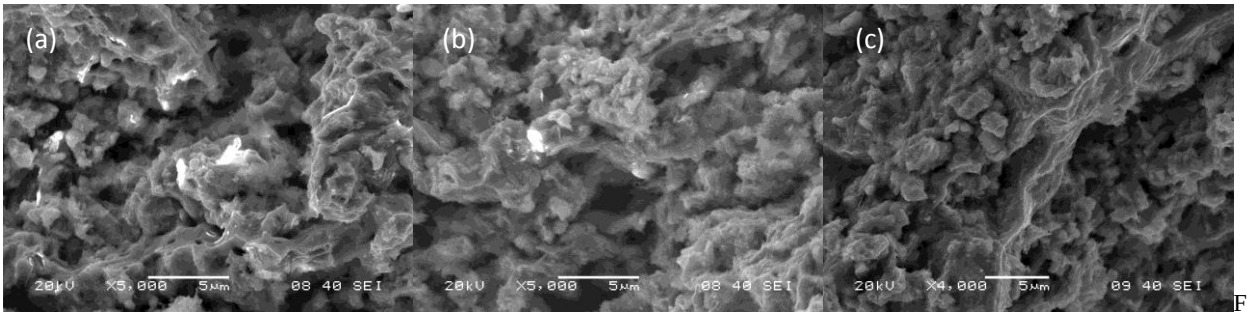

Fig:4.25 SEM micrograph illustrating the thermal shocked 3-point bend test specimen fracture surface of nanocomposites (a)no treatment (b) up-thermal shock (c) down-thermal shock

4.9 Thermal conditioning

4.9.1 Microcomposite

At +80 °C conditioning temperature, the ultimate flexural strength of microcomposite decreases by 29.27% from the untreated sample. At high temperature the internal residual stress (developed due to mismatch of coefficient of thermal expansion) is released by plastic deformation of the matrix rather than by interfacial decohession. As the constraints imposed by expanding elastic matrix it imparts a compressive force on the particle. This phenomenon may be attributed to the particle fragmentation (evidence from SEM micrograph Fig.4.27(b)) which leads to composite softening. The ultra low temperature conditioning at -80°C may impart shrinkage of matrix which causes interface decohesion (evidence from SEM micrograph Fig. Fig.4.27(c)). So the strength of a microcomposite decreases by 0.93%.

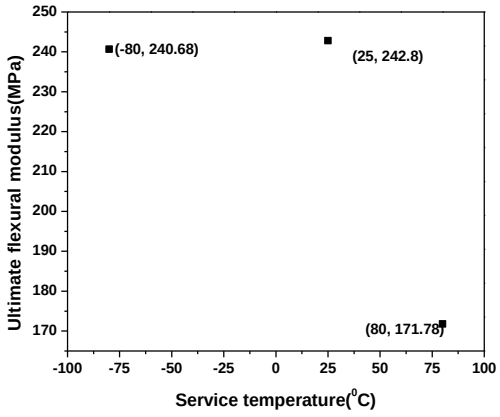

Fig. 4.26 Plot for ultimate flexural stress (MPa) verses thermal conditioning temperature for microcomposite

At low temperature the contraction of matrix is more likely to be a dominant phenomenon than reinforcement particle shrinkage. As the probability of particle cracking decreases, this results in decrease in the detrimental softening effect. So decrease in ultimate flexural strength is less likely to be pronounced as compared to the +80°C conditioning.

Farctography of the thermal conditioned microcomposites

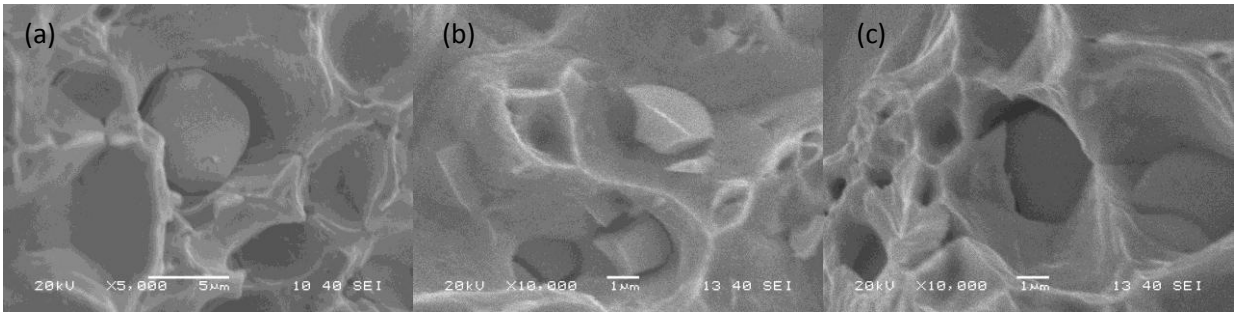

Fig:4.27 SEM micrograph illustrating the thermal conditioned 3-point bend test specimen fracture surface of microcomposites (a)No conditioning (b) Conditioning at +80°C, (c) Conditioning at -80°C

4.9.2 Nanocomposite

At +80 °C, for nano composite the ultimate flexural strength increased by 15.60 % from the untreated sample. This can be explained further as the thermal misfit dislocations which are the gometrically necessary dislocation can operate at high temperature. The nano alumina particles impede the dislocation motion leading to the dislocation pileups at reinforcement particle-matrix interface, which leads to strain hardened the composite. The fracture surface reveal that (Fig. 4.29(b)-(c)) plastically yielding of the matrix and crack bridging are the predominant phenomenon which increases the strength of the composite. On the contrary the ultra low

conditioning of the nanocomposite at -80 °C decreses the composite strength by 26.31%. At low temperature (–80°C) strain hardening exponent decreases with lowering in service temperature because the Peierls stress (stress necessary to move a dislocation) is very high. As movement of dislocation is a temperature driven phenomena, at low temperature movement of dislocation is arrested which restrict the dislocation pile up consequently decreasing the density of dislocation forest.

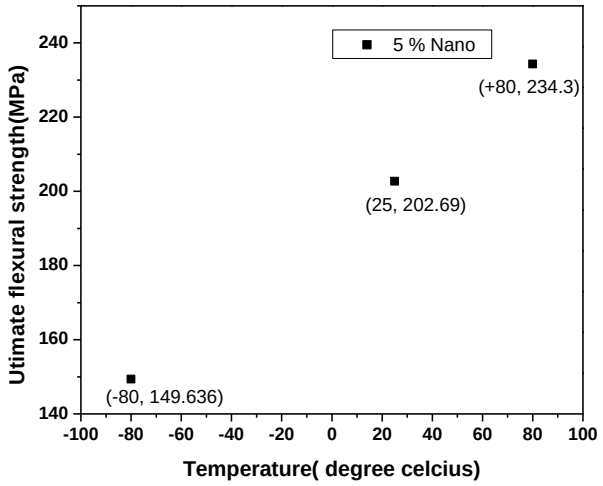

Fig. 4.28 Plot for ultimate flexural stress (MPa) verses thermal conditioning temperature for nanocomposites

Fractography of the thermal conditioned nanocomposites

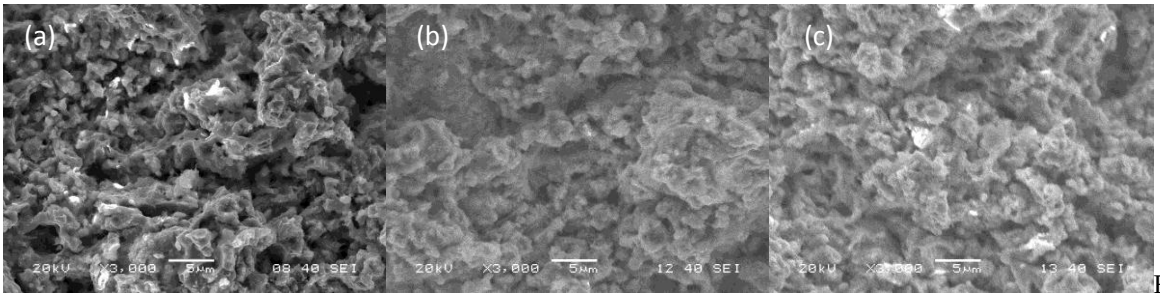

Fig:4.29 SEM micrograph illustrating the thermal conditioned 3-point bend test specimen fracture surface of nanocomposites (a)No conditioning (b) Conditioning at +80°C, (c) Conditioning at -80°C

4.10 In-situ high temperature 3-point bend test

4.10.1 Microcomposite

In case of micro composite at 100°C copper matrix expand elastically. The metal and ceramic phase of the composite develops tensile and compressive stress respectively [64] compressive stress builds up on the particle due to expansion of the Cu matrix. Matrix imposed a compressive force on the particle which increases the interfacial physical proximity (illustrate in fig:4.31(b)) between matrix and reinforced particle. This leads to the direct strengthening of the composite as a result ultimate flexural strength of the composite increases by 18.12% from the room temperature test value.

At 250°C service temperature the ultimate flexural strength values decreases by 20.56% from the room temperature test value. At higher operating temperature plasticity of the composite increases due to (1) dislocation annihilation (2) activation of dislocation motion by different mechanism other then glide(3) relaxation of internal stress at the matrix-particle interface, (4) enhancement of dislocation recovery at the interface.[23] and (5) grain coarsening of the matrix by the application of applied load. All the above stated phenomena decrease the strength hardening exponent of the composite leading to decrease in ultimate flexural strength of the composite. The fractography study (revealed from fig. 4.31(c)) confirms that the composite fails through the plastic deformation of the matrix and matrix folding.

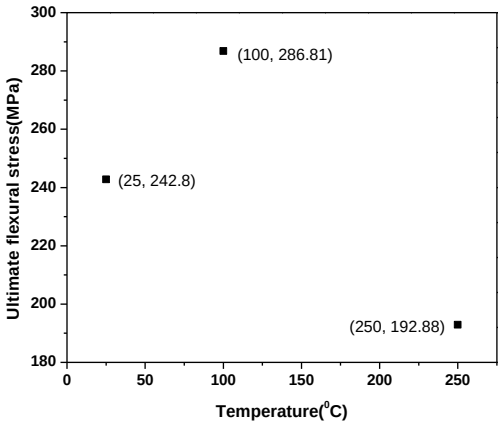

Fig. 4.30 Plot for ultimate flexural stress (MPa) verses service temperature for in-situ 3-point bend test specimen of microcomposites

Fractography of in-situ treated microcomposites

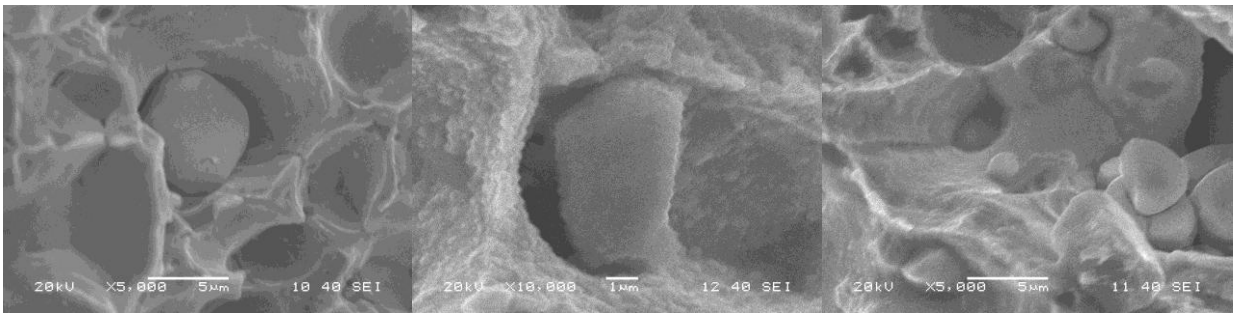

Fig. 4.31 Fractography of the in-situ 3-point bend test samples (a) room temperature, (b)thermal treatment at 100°C and (c) thermal treatment at 250°C of microcomposites.

4.10.2 Nanocomposite

With incresee in operating temperature the strength of the nanocomposite decrease by 1.08 % at 100°C and 20.05% at 250°C service temperature. With increase in operating temperature the strengthening mechanisms that operate at lower temperature get relaxed[64] which decrease the strength of the composite. The fractography study reveals that the the fracture mode of the composite at 100°C is brittle type due to the presence of river line mark (Fig.4.33(b)) whereas the failure of the composite at 250°C occur by matrix cracking(Fig.4.33(c))

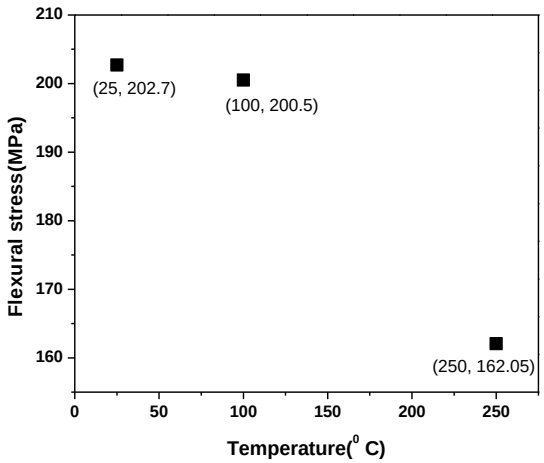

Fig. 4.32 Plot for ultimate flexural stress (MPa) verses service temperature for in-situ 3-point bend test specimen of nanocomposites

Fractography of in-situ treated microcomposites

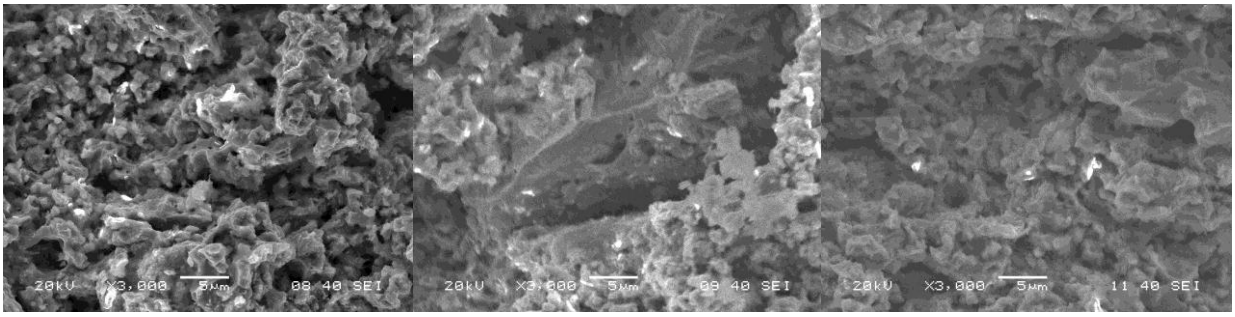

Fig. 4.33 Fractography of the in-situ 3-point bend test samples (a) room temperature, (b)thermal treatment at 100°C and (c) thermal treatment at 250°C of nanocomposites.

Chapter 5
Conclusions

Conclusion

- ✓ Cu-Al_2O_3 micro and nano composites were fabricated by conventional powder metallurgy route.
- ✓ XRD analysis confirms the presence of Cu, Cu_2O, Al_2O_3 phases in both micro and nano composites, the amount of cuprous oxide being higher at higher sintering temperatures.
- ✓ Distribution of alumina is better in nanocomposites as compared to microcomposites. With increases in volume fraction of reinforcement nanoparticles, they tend to agglomerate.
- ✓ Density and microhardness values for nanocomposites are maximum for lower sintering temperature i.e. at 850˚C, where as for microcomposite the density and microhardness values are maximum at higher sintering temperature.
- ✓ Nanocomposites are more resistant to wear. As the alumina content increases the wear resistance of both micro and nano composite increases.
- ✓ The compression strength of nanocomposites is higher than of microcomposites.
- ✓ 3-point bend test infer that flexural modulus is higher for nanocomposites than microcomposite.
- ✓ Both up and down thermal shock treatments enhance the ultimate flexural strength of microcomposites.
- ✓ Thermal conditioning of nanocomposites at +80˚C improves ultimate flexural strength.
- ✓ At high operating temperatures (i.e. 100˚C, 250˚C) ultimate flexural strength of nanocomposite decreases.

1. S.F. Moustafa, Z.Aa Hamid, A.M. Elhay, Mater. Lett. ;53(002) 224–229.

2. H. Wanga, R. Zhanga, X. Hua, C.A. Wangb, Y. Huangb, Mater. Process. Technol. 197(2008)43–48.

3. G.E. Dieter, Mechanical Metallurgy, third ed., McGraw- Hill, London, United Kingdom, 1988.

4. D.J. Lloyd, Int. Mater. Rev. 39 (1994) 1-23.

5. G. O. Donnell, L. Looney, Mater. Sci. Eng. A 303(2001) 292- 301.

6. S. Sivasankaran, K. Sivaprasad, R. Narayanasamy, VK Lyer, Powder. Technol, 201(2010)70-82.

7. G. C. Efe, I. Altinsoy, T. Yener, M. Ipek , S. Zeytin, C. Bindal. Vacuum 85(2010)643–647.

8. D. B Miracle, Compos. Sci. Technol. 65 (2005) 2526-2540.

9. M. Korac, Z. Kamberovic, M. Tasic, M. Gavrilovski, Chem. Ind. Chem. Eng. Q 14 (2008) 215-218.

10. G. C. Efe, S. Zeytin, C. Bindal, Mater. Des. 36(2012)633-663.

11. W. Tong, G. Ravichandran , Compos. Sci. Technol. 52 (1994) 247-252.

12. L. Lu, M.O.Lai, G. Li, Mater. Res. Bull. 31 (1996) 453-464.

13. K. Dash, B.C. Ray, D. Chaira, J. Alloys. Compd. 516(2012) 78-84.

14. I.J. Shon, J.Y. Lee, K.S. Nam, Electron. Mater. Lett.5 (2009) 77-81.

15. J. Ye, B.Q. Han, Z. Lee, B. Ahn, Scripta Mater. 53 (2005) 481-486.

16. Y. Tanaka, J.M. Yang, Y.F. Liu, Y. Kagawa, Scripta Mater. 56(2007) 209-212

17. A. Kelly, C. Zweben, Comprehensive Composite Materials 3, first ed., Elsevier Science Ltd., United Kingdom, 2000.

18. D.B Miracle, S.L. Donaldson, Introduction to composite IN ASM handbook editors: composites, vol. 21, materials park: ASM international: 2001, 3-17.

19. Karl U. Kainer, Custom-made Materials for Automotive and Aerospace Engineering. Copyright © 2006 WILEY-VCH Verlag GmbH & Co. KGaA, Weinheim ISBN: 3-527-31360-5

20. R.M. German, Sintering Theory and Practice. 1 ed. 1996, New York: John Wiley & Sons.

21. S.H. Goods , L.M. Brown, Acta metall. 27(1979)1-15.

22. T. A. Kharaishi, L. Yan, Y.L. Shen, Int. J. Plast. 20 (2004)1039- 1057.

23. M.Taya, K.E. Lulay, D.J.Lloyd, Acta Metal. Mater. 39 (1991) 73-87.

24. K.Rajkumar, S.Aravindan, J. Mater. Process. Technol. 209 (2009)5601-5605.

25. C. Suryanarayana, Int. Mater. Rev. 40 (1995) 51-53.

26. D.J. Lloyd, Acta Metal. Mater. 39(1991)59-71.

27. P. Ganguly, W.J. Poole, D.J. Lloyd, Scripta Mater. 44(2001)1099-1105.

28. J. Gurland, I.J. Plateau, Trans. Am. Soc. Metals. 56, (1963) 442.

29. T. F. Klimowicz, K.S. Vecchio, Fundamental relationship between microstructure and mechanical properties of metal matrix composites, Eds P.K. Liaw , M.N. Gungor, TMS, Warrendale, PA, 1990, 255-267.

30. ASM handbook, Fractography, The materials information society, Fractogrphy, vol-12.

31. A.F. Whitehouse, T.W. Clyne, Compos. 3 (1993) 256-261.

32. G. Liu, Z. Zhang, J.K. Shang, Acta Metall. Mater. 42 (1994) 271-280.

33. T.W. Clyne, P.J. Withers, An Introduction to Metal Matrix Composites, first ed., Cambridge University Press, Cambridge, 1993.

34. L. Zhang, X.B. He, X.H. Qu, X. Lu, M.L. Qin, Wear. 265 (2008)1848- 1856.

35. B. Cornwall, V. D. Krstic, J. Mater Sci. 27 (1992) 1217.

36. M. Kubota , P. Cizek, W.M. Rainforth Compos Sci. Technol. 68(2008) 888-895.

37. X. L. Zhong, W. L. E. Wong, M. Gupta, Acta materialia 55(2007) 6338-6344.

38. L. Lu, M.O. Lai, G. Li Mater. Res. Bull. 31,(1996) 453-464.

39. R.W. Hertzberg, Deformation and fracture mechanics of engineering materials, Wiley, New York, 1996, 66.

40. A.A. Mazen, J. Mater. Eng. Perf. 8(1999) 487-495.

41. D. Zhao, F.R. Tuler, D.J. lloyd, Acta metall mater.42, (1994)2525.

42. F. Shehata, A. Fathy, M. Abdelhameed,S.F. Moustafa, J. Alloys Compd., 476 (2009) 300-305.

43. R. Ritasalo, X. W. Liu, Procedia Engineering 10(2011)12-129.

44. M. Barmouz, M. K. B. Givi, J. Seyfi, Mater. Charact. 62(2011)108-117.

45. Z. Jianhua, L. L.B. Shen, W. Hu, Mater. Lett. 61 (2007) 2804–2809.

46. A. Levy, M. Papazian , Acta Mtall Mater 39(1991)2555.

47. E.U. Lee, Metall. Trans. 23(1992) 2205.

48. Y. D.Haung. N. Hort, Int. J. Fatigue 28(2006) 1399-1405.

49. P. Agrawal, C.T. Sun, Compos Sci. Technol. 64 (2004) 1167-1178

50. P Agrawal, K. Bowman, CT Sun. Acta Mater. 51(2003)1143-1156.

51. S. F. Hassan, M. Gupta. Mater. Sci Eng. A, 392(2005)163-168.

52. H. Ghasemi, M.A.F. Sani, A.H. Kokabi, Z. Riazi. Mech. Eng. Trans. B 216(2009)263-268.

53. G. C. Efe, T. Yener, I. A. ltunsoy, M. Ipek, S. Zeytin, C. Bindal, J. Alloys. Compd. 509(2011) 6036-6042.

54. A. Slipenyuk, V. Kuprin, Yu. Milman, V. Goncharuk, J. Eckert Acta Mater. 54 (2006) 157-166.

55. S. Suresh, A. Mortensen, A. Needleman, Fundamentals of Metal-Matrix Composites. Butterworth- Heinemann; 1993.

56. C. Scheu, M. Gao, S.H. Oh, G. Dehm, J. Mater. Sci. 41 (2006) 5161-5168.

57. V. Rajkovic, D. Bozic, M.T. Jovanovic Mater. Des. 31(2010)1962-1970.

58. V. Rajkovic, D. Bozic, M. T. Jovanovic, J. Mater. Process. Technol. 200 (2008) 106-114.

59. F. Shehata, A. Fathy, M. Abdelhameed, S.F. Moustafa, Mater. Des.30 (2009) 2756–2762.

60. C. S. Ramesh, R. Noor Ahmed, M. A. Mujeeb, M. Z. Abdullah Mater. Des. 30(2009)1957–1965.

61. S.F. Hassan, M. Gupta, Mater. Sci. Tech. 19 (2003) 253–259.

62. Q.B. Nguyen, M. Gupta, Comp. Sci. Tech. 68 (2008) 2185–2192.

63. Z. Szaraz, Z. Trojanova, M. Cabbibo, E. Evangelista, Mater. Sci. Eng. A 462 (2007) 225–229.

64. E. Martin, A. Forn, R. Nogue, J. Mater. Proces. Technol.143-144(2003)1-4.